


Article

Co-Design of CVT-Based Electric Vehicles

Caiyang Wei ^{1,*} , Theo Hofman ¹  and Esin Ilhan Caarls ^{1,2}

- ¹ Department of Mechanical Engineering, Eindhoven University of Technology, P.O. Box 513, 5600 MB Eindhoven, The Netherlands; t.hofman@tue.nl (T.H.); Esin.IlhanCaarls@nl.bosch.com (E.I.C.)
² Bosch Transmission Technology, Postbus 500, 5000 AM Tilburg, The Netherlands
* Correspondence: c.wei.1@tue.nl; Tel.: +31-40-247-8325

Abstract: For an electric vehicle (EV) with a continuously variable transmission (CVT), a novel convex programming (CP)-based co-design method is proposed to minimize the total-cost-of-ownership (TCO). The integration of the electric machine (EM) and the CVT is the primary focus. The optimized system with co-design reduces the TCO by around 5.9% compared to a non-optimized CVT-based EV (based on off-the-shelf components) and by around 2% compared to the EV equipped with a single-speed transmission (SST). By taking advantage of the control and design freedom provided by the CVT, the optimal CVT, EM and battery sizes are found to reduce the system cost. It simultaneously finds the optimal CVT speed ratio and air-flow rate of the cooling system reducing the energy consumption. The strength of co-design is highlighted by comparing to a sequential design, and insights into the design of a low-power EV that is energy-efficient and cost-effective for urban driving are provided. A highly integrated EM-CVT system, which is efficient, low-cost and lightweight, can be expected for future EV applications.

Keywords: electric vehicle; co-design; continuously variable transmission; component sizing; optimal control; convex programming; energy efficiency



Citation: Wei, C.; Hofman, T.; Ilhan Caarls, E. Co-Design of CVT-Based Electric Vehicles. *Energies* **2021**, *14*, 1825. <https://doi.org/10.3390/en14071825>

Academic Editor: João Pedro Trovao

Received: 11 February 2021

Accepted: 19 March 2021

Published: 25 March 2021

Publisher's Note: MDPI stays neutral with regard to jurisdictional claims in published maps and institutional affiliations.



Copyright: © 2020 by the authors. Licensee MDPI, Basel, Switzerland. This article is an open access article distributed under the terms and conditions of the Creative Commons Attribution (CC BY) license (<https://creativecommons.org/licenses/by/4.0/>).

1. Introduction

Growing concerns of environmental contamination and depletion of natural resources have led to the resurgence of electric vehicles (EVs). Admittedly, the emerging EV market is mainly dominated by single-speed transmissions (SSTs). Nevertheless, to optimize key performance indicators (KPIs), for example, energy consumption, system cost and performance, research on multi-speed transmissions is gaining popularity, such as two-speed transmissions and continuously variable transmissions (CVTs) [1–4].

To date, design of EVs (including CVT-based) is largely based on off-the-shelf components due to cost, and powertrain components are typically not optimized [5]. The component size, for example, the electric machine (EM) size in kW and battery size in kWh, is associated with the component cost. Finding optimal component sizes would contribute to cost reduction. The component size also influences the vehicle performance, such as top speed and acceleration time. Moreover, EV energy consumption is largely influenced by the driveline efficiency. In this respect, the integration of the EM and the CVT plays a key role [6]. The CVT could provide opportunities of optimizing the EM, thanks to the continuous ratio adjustment functionality. The wider power availability of the EM, in turn, could offer opportunities of optimizing the CVT. In literature, however, the EM and the CVT are often treated independently. Standard CVT controllers developed for conventional vehicles are used, where the speed ratio of the CVT (control) is selected to reduce the EM power losses. The influence of the CVT efficiency, CVT and EM size (design) are not always considered simultaneously [4]. In order to maximize system efficiency and minimize system cost, the coupling between the EM and the CVT from design and control perspectives has yet to be investigated. In order to address these issues, design and control frameworks are required.

This type of design problem can be tackled by different approaches. An overview of design and control optimization methodologies is given in [7,8]. As presented in [7], there are generally four approaches to solve the design (plant) and control (controller) problem. With respect to solution optimality, simultaneous and nested coordination schemes outperform iterative and sequential ones, although depending on the coupling and how sensitive the solution is to uncertainties in the design parameters. For instance, the optimal component sizes can be found iteratively, by using rule-based control [9]. However, these methods do not guarantee a globally optimal solution. To overcome this limitation, dynamic programming (DP), as an optimization-based strategy, can be used to find the optimal control inputs [10]. DP can also be utilized in combination with an evolutionary algorithm to find component sizes, such as particle swarm optimization (PSO). In the search space, PSO improves a candidate solution iteratively by moving particles towards the best known positions [11,12]. It can solve complex objective functions and problems with large design space. PSO is used in [13] to find optimal component sizes of an electrified powertrain. However, it requires tuning effort and has long computation time. Furthermore, an optimal solution is not guaranteed. An alternative is to use convex programming (CP) as a simultaneous approach, which is also a co-design optimization method. It finds optimal design parameters and control trajectories simultaneously without the need of checking optimality [14,15]. It ensures a unique optimum with a convex objective function and a convex feasible region. It is also computationally efficient. Due to the low computation time, CP enables optimization of problems with many dynamic states, such as thermal states, which may not be tractable by using DP for example [16].

Moreover, employing a CVT for an EV is a novel concept. Applying advanced optimization methods to optimize KPIs of CVT-based EVs have hardly been found [6]. Additionally, current research mainly concentrates on the energy domain to increase the energy efficiency, taking into account the mechanical and electrical energy flows [17]. The thermal domain, however, for instance, evaluation of cooling power consumption and temperature profile, has yet to be explored. It is also an integral part of an EV, which would affect the total energy consumption [18].

Considering the integration of the EM and CVT, as shown in Figure 1, the CVT speed ratio over time (γ_v) for a use case changes the EM and CVT operating points. Therefore, it influences the EM ($P_{m,loss}$) and CVT ($P_{c,loss}$) power losses. Furthermore, the desired CVT speed ratio affects the CVT size (s_γ), for example, the ratio coverage of the CVT, and the EM size (s_τ) to meet the power demand for example. The CVT and EM sizes are related to their costs. The CVT size that determines the ratio range, in turn, affects the CVT speed ratio and the EM size. The EM size also has an effect on the CVT size and its speed ratio. In addition, the component size affects its own efficiency. Moreover, the battery size and losses are affected indirectly. Hence, the hypothesis is that there exists an optimal combination of the CVT speed ratio over time, battery size, EM size and the CVT size for an application, which results in the lowest total-cost-of-ownership (TCO). TCO consists of energy consumption and system cost. The system cost comprises the CVT, EM (including inverter) and battery prices. Given the interactions between these variables, this optimal solution for a use case can best be found by means of a simultaneous approach in an efficient manner.

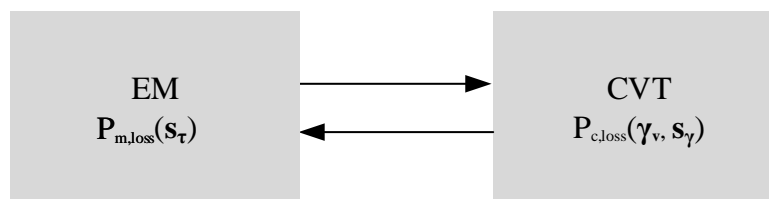


Figure 1. Schematic representation of the coupling between the continuously variable transmission (CVT) and electric machine (EM), where γ_v represents the CVT speed ratio, s_γ the CVT size, s_τ the EM size, $P_{c,loss}$ the CVT power losses, and $P_{m,loss}$ the EM power losses.

Motivated by the above discussion, this study originally proposes a CP-based co-design optimization strategy for a CVT-based EV to reduce the TCO. It identifies the optimal CVT speed ratio over time and the desired air-flow rate of a thermal management system (TMS) to maintain the EM temperature below its thermal limit. Furthermore, it finds the optimal sizes of the CVT, EM and battery. The approach is as follows:

- S_1 : An SST-based EV model including energy dynamics and thermodynamics with reference to a series production vehicle is firstly created. It is developed based on static efficiency maps represented by lookup tables, which is validated against measurement data from real-world driving. It replicates the physical behavior of the vehicle in reality.
- S_2 : A CVT-based EV model is then developed based on S_1 , where only the SST is replaced by a CVT (an off-the-shelf component, which is not optimized). Other components, for example, the battery and EM, are the same. The CVT model is created based on experimental data from a test rig.
- S_3 : Component models from S_2 are convexified to fit the measurement data from real-world driving and experimental data from the test rig. S_2 is subsequently optimized with the co-design optimization strategy.

All the systems (S_1 , S_2 and S_3) have the same maximum EM power and similar vehicle performance (i.e., 0–100 km/h acceleration time below 11 s, top speed above 165 km/h, gradability above 30%). Therefore, the goal of this study is to show the advantages of the co-design approach in optimizing a CVT-based EV (e.g., sizing) and to compare TCO between S_1 , S_2 and S_3 . System cost comprising the expenses of the battery, EM and CVT are solely given for the implementation of the co-design approach. Moreover, the strengths of the co-design method are highlighted, by comparing with a sequential approach, where the EM size is fixed to meet performance requirements. Additionally, for urban driving that does not require high performance, insights into the design of a low-power EV are provided.

2. Problem Definition

The configuration of the considered EV is demonstrated in Figure 2. The integration of the EM and the CVT is the primary focus, which are highlighted in bold. The major components of the EV are the battery, DC (direct current)-DC converter, DC-AC (alternating current) inverter, EM, CVT, electric oil pump (EOP), and vehicle. If not specified, the DC-AC inverter and EM are combined together in this study. The final drive (FD) that takes a constant value and a fixed efficiency is lumped into the variator (VA), which together is regarded as CVT. In order to change the CVT speed ratio, hydraulic actuation power is required from the EOP. The EOP power is supplied by the DC-DC converter onboard, which is assumed to be always charged. The EM is directly connected to the input shaft of the CVT without a pre-reduction gear. The battery provides the power requested by the EM. The EV model describes the longitudinal dynamics. It is backward-facing, that is, the drive cycle is given, with a discrete time-step of one second using time index k . The vehicle inertia is considered. The main model parameters are listed in Table A1 (Appendix D), including vehicle parameters and validated thermal parameters.

The main design criterion to find the optimal control and design variables is the minimization of the TCO, which consists of the consumed electricity cost J_e and system cost J_s , given by

$$\min_{s, \mathbf{x}(k), \mathbf{u}(k)} J_e(\mathbf{s}, \mathbf{x}(k), \mathbf{u}(k) | w(k)) + J_s(\mathbf{s} | w(k)), \quad (1)$$

$$\text{s.t. } \mathbf{x}(k+1) = \mathbf{x}(k) + \mathbf{f}(\mathbf{s}, \mathbf{x}(k), \mathbf{u}(k), w(k)) \Delta t, \quad (2)$$

$$\mathbf{h}(\mathbf{s}, \mathbf{x}(k), \mathbf{u}(k)) = 0, \quad (3)$$

$$\mathbf{g}(\mathbf{s}, \mathbf{x}(k), \mathbf{u}(k)) \leq 0, \quad (4)$$

where Δt is the time step. The design variables s consist of the ratio coverage of the CVT s_γ , the scaling factor s_τ for scaling the maximum EM torque and the scaling factor s_b for scaling the battery cells, that is,

$$s = [s_\gamma, s_\tau, s_b]^T. \tag{5}$$

The state variables $x(k)$ are the state-of-energy of the battery and temperature states of the TMS, which are described in Section 3.7, given by

$$x(k) = [E_b(k), \theta_m(k), \theta_c(k), \theta_o(k), \theta_i(k)]^T. \tag{6}$$

The control variables $u(k)$ are the speed ratio of the CVT (γ_v) and the air-flow rate of the TMS (ϕ_a) to keep the EM temperature below its prescribed thermal limit, that is,

$$u(k) = [\gamma_v(k), \phi_a(k)]^T. \tag{7}$$

The power balance of the vehicle is represented by (3), and (4) represents the feasible design space, where the design, state and control variables are bounded. Equation (4) also represents the component limits. The disturbance vector $w(k)$ contains vehicle speed (v_v) and acceleration (a_v), which are prescribed by the drive cycle, given by

$$w(k) = [v_v(k), a_v(k)]^T. \tag{8}$$

The consumed electricity cost J_e over the drive cycle represented by $w(k)$ starting at $k = 1$ and ending at $k = N$ is obtained by

$$J_e(s, x(k), u(k)) = \sum_{k=1}^N \rho_e P_b(s, x(k), u(k)) \Delta t, \tag{9}$$

where ρ_e is the price of electricity (€/kWh). The term $P_b(s, x, u)$ represents the battery output power. The system cost J_s over the drive cycle is calculated by

$$J_s(s) = \frac{S_d}{S_v} (C_c(s_\gamma) + C_m(s_\tau) + C_b(s_b)), \tag{10}$$

where S_d is the length of the drive cycle (km) and S_v the traveled distance of the vehicle in its lifetime. The variable $C_c(s_\gamma)$ represents the CVT cost, $C_m(s_\tau)$ the EM cost (including inverter) and $C_b(s_b)$ the battery cost.

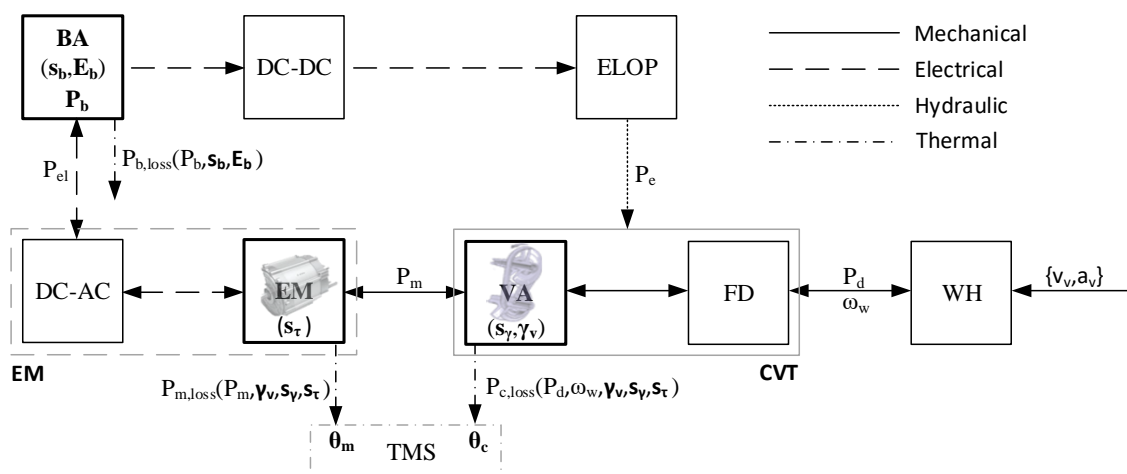


Figure 2. A CVT-based electric vehicle, where BA represents the battery, DC-AC the DC (direct current) to AC (alternating current) inverter, DC-DC the DC to DC converter, ELOP the electric oil pump, FD the final drive, VA the variator, and WH the wheel. Design, control, and state variables are highlighted in bold.

Based on the configuration shown in Figure 2, three systems, namely S_1 , S_2 and S_3 , are developed and compared in terms of TCO as in (1). Three systems have the same battery. Although battery aging is not the focus of this study, the methodology presented also applies to scenarios where battery needs to be changed. S_1 is developed with reference to the series production vehicle, which is described in Appendix A. S_2 is created based on S_1 , where only the SST is replaced by the CVT, which is presented in Appendix B. In S_1 and S_2 , the component models are represented by experimentally-based lookup tables (efficiency maps), which describe the power generation or power dissipation of each component. The design variables are fixed. In S_2 , the CVT speed ratio is predetermined by a low-level CVT controller, which is developed based on [19]. The goal of the CVT controller is to reduce the EM power losses depending on the power demand, which is common in literature, such as [20]. The air-flow rate of the TMS is tuned to maintain the EM temperature below its thermal limit. In S_3 , convex models are developed based on measurements. The design and control variables are to be determined by the co-design optimization strategy.

This section formulates the co-design optimization problem of a CVT-based EV. To solve this co-design optimization problem, the required convex EV model based on measurements, especially the mathematical coupling between the CVT and EM from design and control perspectives, is presented in more detail in the next section.

3. System Modeling

This section presents the convex EV model and cost models needed for solving the co-design problem defined in (1). An introduction to CP is first given in Appendix C, which serves as a guideline for developing convex models. A data-driven approach used to derive the convex models is then provided in Section 3.1. Subsequently, given the drive cycle in Section 3.2, the vehicle longitudinal dynamics are described in Section 3.3, which is an input to the convex models in S_3 . Given the input, however, the torque input to the CVT is not available. Because the CVT speed ratio is a control variable, which is not known in advance and will be determined by the co-design optimization strategy. Dealing with torque information will lead to non-convexity (Appendix C). Therefore, to preserve convexity for the co-design optimization problem, all the relations are converted to power level. By utilizing the data-driven approach as mentioned above, three convex models are consequently developed, namely the CVT power loss model (Section 3.4), EM power loss model (Section 3.5) and the EM power limitation model (Section 3.6). Equality constraints are also relaxed with inequalities where applicable, and the equality holds at the optimum. Notice that, this study mainly focuses on the CVT, EM and battery sizing, and the ELOP sizing is not required at this level. Therefore, the ELOP is only considered in the calculation of energy consumption, and no convex representation is required. The ELOP power losses are computed offline, meaning the ELOP power losses are obtained based on the optimal CVT speed ratio found by the optimization algorithm and then added to the energy consumption. Furthermore, to remove the heat (power losses) generated by the EM and CVT, the TMS and its associated thermal model are presented in Section 3.7. Eventually, the required power is supplied by the battery, which is described in Section 3.8. The convex battery model is developed based on physics [21]. Additionally, in Section 3.9, convex mass and cost models related to CVT, EM and battery sizes are developed for the implementation of the co-design approach.

3.1. Derivation of Convex Models

As mentioned in Appendix C, the component models, for example, the power loss models, are required to be convex for the CP algorithm. The general idea to derive the convex models based on a data-driven approach can be seen in Figure 3, where measurements are used as inputs for the modeling. The measurement data (top) about the CVT and EM, for example, power losses, torque, speed, and ratio over time, are first served as inputs. Based on these measurements, a set of convex expressions capturing input and

output relationships with sufficient accuracy is created. With different combinations of those expressions, for example, CVT and EM power loss models, are then developed. These parameterized models are subsequently fitted to capture the loss behaviors of components with sufficient accuracy, which have a negligible impact on the result. Fourth, the convex models are utilized by the co-design optimization method to find the optimal solution of the system.

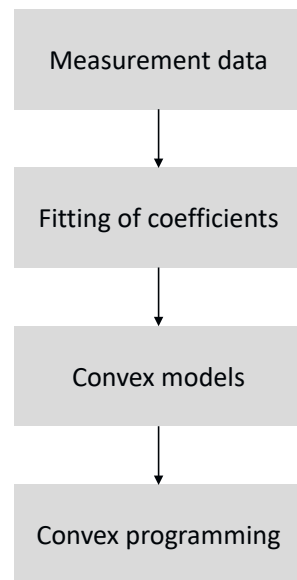


Figure 3. A data-driven approach to derive convex models. In order to apply convex programming, constraints and cost function are also required to be convex.

3.2. Drive Cycle

In this work, a realistic and representative real-world drive cycle, Worldwide Harmonized Light Vehicles Test Cycles (WLTC), is chosen. It is currently widely adopted in the automotive sector to certify energy consumption. It includes low, medium, high, and extra high speed scenarios, which can represent, for example, urban, rural, and highway driving conditions. In order to show the thermal effect, two repeated WLTC is used. The drive cycle contains the vehicle speed $v_v(k)$ and acceleration $a_v(k)$. Note that, although the quantity (e.g., energy consumption) might vary, the methodology presented also applies to other drive cycles.

3.3. Longitudinal Dynamics

Note that, in this case the total vehicle mass is a variable because of the scaling factors for the CVT, EM and battery, which will be presented in the next sections. Considering all the forces acting on the vehicle, the power demand for the known WLTC can be obtained by

$$P_d(k) = \left(\frac{1}{2} \rho_a c_d A_f v_v^2(k) + c_r m_v g \operatorname{sign}(v_v(k)) + \left(m_v + 4 \frac{J_w}{r_w^2} \right) a_v(k) \right) v_v(k), \quad (11)$$

where the total vehicle mass m_v is given by

$$m_v = m_{cw} + m_c + m_m + m_b + m_d, \quad (12)$$

where m_{cw} is the curb weight excluding the CVT (m_c), EM (m_m) and battery (m_b) mass (Table 1). m_d is the driver mass.

Table 1. Comparison of component parameters between S_1 , S_2 and S_3 .

Parameter	Unit	S_1	S_2	S_3
Transmission ratio	-	9.02	[4.47, 16.8]	[3.5, 11.68]
EM scaling factor	-	1	1	0.79
Battery cells	-	264	264	253
Maximum EM torque	Nm	290 ($\bar{\tau}_m$)	290	228
EM base speed	rpm	3293 ($\omega_{m,b}$)	3293	4188
Maximum EM power	kW	100 (\bar{P}_m)	100	100
Curb weight	kg	1252 (m_{cw})	1252	1252
Transmission mass	kg	26 (m_s)	56 (\bar{m}_c)	52
EM mass	kg	74 (\bar{m}_m)	74	58
Battery mass	kg	318 (\bar{m}_b)	318	303
Driver mass	kg	90 (m_d)	90	90

3.4. Convex CVT Model

Convex modeling of the CVT is shown in Figure 4, taking into account the effect of design (s_γ, s_τ) and control (γ_v) on the CVT power losses ($P_{c,loss}$).

Based on the measurement data, the CVT torque losses $\tau_{c,loss}$ can be expressed as a function of its input torque τ_c , input speed ω_p , and ratio over time γ_v . As shown in Figure 2, the relationships in S_3 are converted to the power domain. At given input speeds to the CVT, the CVT torque losses $\tau_{c,loss}$ are converted to their corresponding power losses $P_{c,loss}$, that is,

$$P_{c,loss}(k) = \tau_{c,loss}(k) \omega_p(k). \tag{13}$$

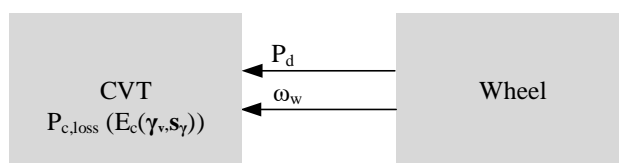
On the basis of these inputs (τ_c , ω_p , and γ_v) to the CVT, the outputs (P_d and w_w) of the CVT can be determined as

$$P_d(k) = \tau_c(k) \omega_p(k) - P_{c,loss}(k), \tag{14}$$

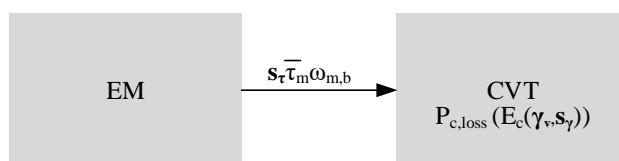
$$w_w(k) = \frac{\omega_p(k)}{\gamma_v(k)}. \tag{15}$$

The input-output relationship of the CVT implies that the CVT power losses can also be formulated on system level as (Figure 4a):

$$P_{c,loss}(k) = P_{c,loss}(P_d(k), w_w(k), \gamma_v(k)). \tag{16}$$



(a) Effect of design (s_γ) and control (γ_v) on the CVT power dissipation



(b) Effect of EM design (s_τ) on the CVT power dissipation

Figure 4. Convex modeling of the CVT, where $\bar{\tau}_m$ represents the maximum EM torque and $\omega_{m,b}$ the EM base speed.

Clearly, the CVT power dissipation is influenced by the control variable γ_v . However, while P_d and w_w are known here, the CVT speed ratio γ_v will be decided by the optimization algorithm. Dealing with this speed ratio alone would lead to non-convexity (Appendix C). Hence, considering the co-design problem and in order to preserve convexity, the information of γ_v is embedded in another variable E_c , by applying a change of variables [22], given by

$$E_c(k) = \gamma_v^2(k) \omega_w^2(k). \quad (17)$$

Notice that there is no information loss and the optimization strategy will assess every possible combination of γ_v and ω_w . There are also two other reasons of selecting E_c . Firstly, the CVT is a rotating mechanical component, and this term is closely related to its kinetic energy. Secondly, in practice, the CVT speed ratio is often determined based on the EM speed $\gamma_v \omega_w$ and wheel speed ω_w , since there is always torque loss in between, but there is no speed loss. Therefore, the CVT power dissipation is affected by $E_c(\gamma_v)$ (Figure 4a), as it contains the information of speed ratio. Furthermore, the variable $E_c(\gamma_v)$ is influenced by the ratio coverage of the CVT s_γ , which is the range that the CVT can actually shift, as illustrated in Figure 5. In this figure, $\underline{\gamma}_v$ and $\bar{\gamma}_v$ are the overdrive ratio and underdrive ratio of the CVT, respectively. The ratio coverage of the CVT is defined by

$$s_\gamma = \bar{\gamma}_v / \underline{\gamma}_v. \quad (18)$$

The CVT sizing is carried out on the basis of the design variable s_γ , because it is one of the most influencing factors that affect cost, efficiency, drivability, and packaging of CVT and powertrain [6]. Note that there are other factors that affect the variator efficiency and hence the CVT loss, such as the center distance of the pulleys and variator asymmetry. Since this study focuses on system-level representation and there is no pre-reduction between the EM and CVT, these factors are not considered. The underdrive ratio $\bar{\gamma}_v$ and the overdrive ratio $\underline{\gamma}_v$ are known. In order to avoid non-convexity for the co-design problem (Appendix C), the overdrive ratio $\underline{\gamma}_v$ is fixed in this study. Therefore, constraints on γ_v , E_c , and s_γ are

$$\gamma_v(k) \in [\underline{\gamma}_v, s_\gamma \underline{\gamma}_v], \quad (19)$$

$$E_c(k) \in [\underline{\gamma}_v^2 \omega_w^2(k), s_\gamma^2 \underline{\gamma}_v^2 \omega_w^2(k)], \quad (20)$$

$$s_\gamma^2 \in [s_\gamma^2, s_\gamma^2]. \quad (21)$$

The CVT power dissipation in (13) is measured based on an original CVT product (sold on the current market) with a full ratio range of [0.38, 2.63]. Therefore, it has a large ratio coverage, torque capacity ($\bar{\tau}_c$) and power capacity (\bar{P}_c). In case of a CVT with reduced ratio coverage (s_γ), smaller ELOP and on-demand actuation, resulting in a compact and small CVT (superscript “s”) with smaller power capacity (P_c^s), a higher CVT efficiency is expected [6,23]. This higher efficiency potential means a lower power dissipation. Compared with the original CVT power losses $P_{c,loss}$ in (16), this lower power dissipation can be modeled by a multiplier μ_c , which is a function of the EM scaling factor, giving

$$P_{c,loss}^s(k) = \mu_c(s_\tau) P_{c,loss}(k). \quad (22)$$

This multiplier is sensitive to many parameters and technological advances. For example, as reported in [24], the maximum efficiency of the current variator could be above 98%. Notice that, the final drive does not benefit from this loss reduction. Additionally, the current CVT and EM are designed separately, which leads to a mismatch between the specifications. In this work, as shown in Figure 2, the EM is connected to the CVT without a pre-reduction gear. The required CVT torque capacity is determined by the output of the EM $s_\tau \bar{\tau}_m$, as demonstrated in Figure 4b. Here, s_τ , the scaling factor for the EM, is a

design variable, which will be explained in Section 3.5. Thus, the multiplier $\mu_c(s_\tau)$ can be obtained by [23]

$$\begin{aligned} \mu_c(s_\tau) &= 0.7 + 0.3 \frac{\bar{P}_c^s}{P_c} \\ &= 0.7 + 0.3 \frac{s_\tau \bar{\tau}_m \omega_{m,b}}{\bar{\tau}_c \omega_{m,b}} \\ &= 0.7 + 0.3 \frac{s_\tau \bar{\tau}_m}{\bar{\tau}_c}, \end{aligned} \tag{23}$$

where $\bar{\tau}_m$ is the maximum EM torque when $s_\tau = 1$ and $\omega_{m,b}$ is the EM base speed. Similar to [23], this multiplier can be interpreted as a proportional improvement of the more efficient variator, which typically accounts for thirty percent of the total power losses in previous applications.

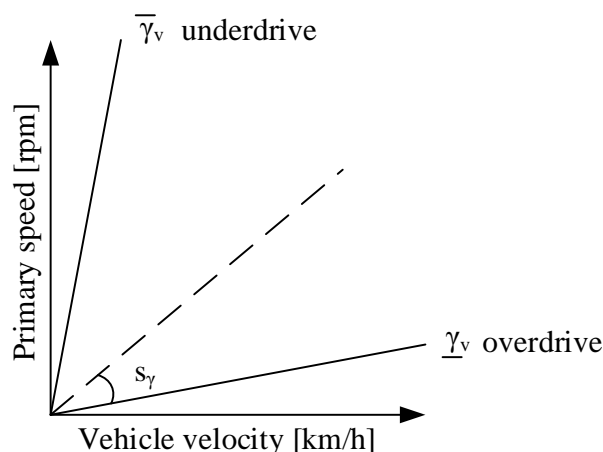


Figure 5. Ratio coverage of the CVT.

Consequently, the factors that influence the CVT power losses are $P_d, w_w, E_c(\gamma_v, s_\gamma)$, and s_τ (Figure 4a,b). Taking into account convexity and possible combinations of expressions, various models are developed to represent the CVT power losses. The models are fitted to capture the loss behavior of the CVT. Based on the evaluated fitting accuracy, the convex CVT model is identified as follows:

$$P_{c,loss}^s(k) = c_{c,0} \left(\frac{P_d(k)}{w_w(k)} \right)^2 + c_{c,1} E_c(k) + c_{c,2} |P_d(k)| + c_{c,3} s_\tau w_w(k) + c_{c,4} s_\tau + c_{c,5}, \tag{24}$$

where $c_{c,0}, c_{c,1}, c_{c,2}, c_{c,3}, c_{c,4}$ and $c_{c,5}$ are the corresponding coefficients. Notice that the power losses are always constrained to be equal to (i.e., vehicle velocity $v_v = 0$) or larger than zero. This model is convex (Appendix C) and has a fitting accuracy of around 98%. It should be noted that, information is exchanged between the terms. For example, the information of s_τ is not only explicitly expressed in s_τ and $s_\tau w_w$, but also implicitly embedded in other terms. The term $s_\tau w_w$ is important for CVT applications, as generally CVT does not operate at very high speeds, yet would lead to lower friction losses of the EM. Another design variable (s_γ) and control variable (γ_v) are reflected in E_c . While the information of speed and torque are conveyed already by $|P_d|$ and $s_\tau w_w$, it is further reinforced by torque squared $(\frac{P_d}{w_w})^2$ and speed squared E_c to capture essential CVT dynamics. An example of $\gamma_v = 0.7$ and $s_\tau = 1$ is shown in Figure 6, where the CVT power dissipation is a function of the power demand and $E_c(\gamma_v, s_\gamma)$. It can be seen that the developed convex CVT model and the original model based on the measurement data resemble well. The difference between them, which is represented by the absolute error, is small for the relevant range. It means that the developed convex model captures the loss behavior of the CVT with

sufficient accuracy. Such correlations in data analysis can be done by clustering the data sets for certain physical attributes. In this case, the CVT power dissipation is considered as the attribute.

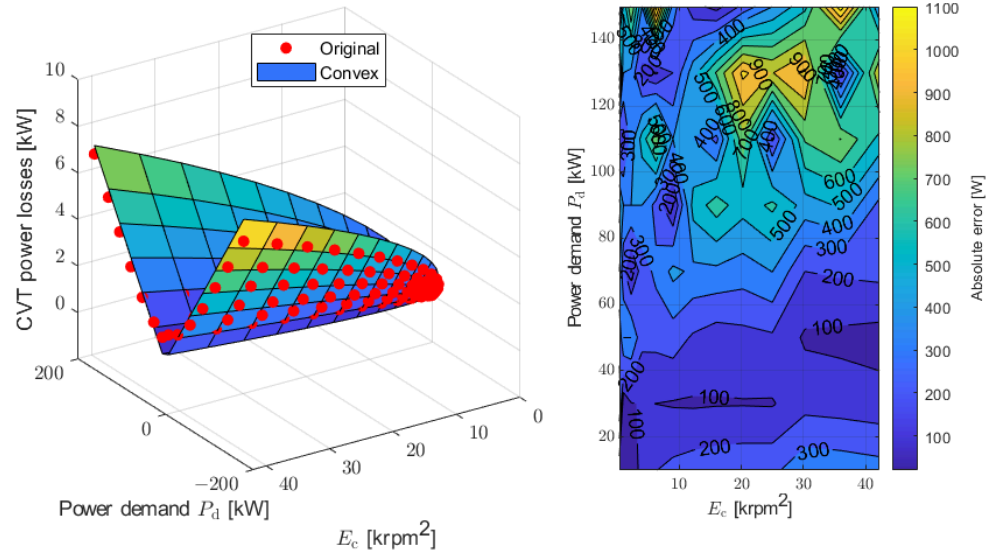


Figure 6. Convex CVT power loss model for $\gamma_v = 0.7$ and $s_\tau = 1$. The absolute error represents the difference in power loss between the convex model and the original model based on the measurement data.

3.5. Convex EM Model

Convex modeling of the EM power losses ($P_{m,loss}$) is illustrated in Figure 7, taking into consideration the interconnections between the EM and CVT from design and control perspectives.

To obtain the convex EM model, the steps in Figure 3 are followed, as it is done for the CVT in Section 3.4. As shown in Figure 2, the EM is directly linked to the input shaft of the CVT and provides the power requested by the CVT, referring to (22), that is,

$$P_m(k) = P_d(k) + P_{c,loss}^s(k). \tag{25}$$

Based on the measurement data, the EM power losses can be expressed as a function of its output torque τ_m and speed ω_m . The EM power dissipation is given by

$$P_{m,loss}(k) = P_{m,loss}(\tau_m(k), \omega_m(k)). \tag{26}$$

On the basis of the output torque and speed of the EM, its output power can be calculated by

$$P_m(k) = \tau_m(k) \omega_m(k). \tag{27}$$

Combing (26) and (27), as depicted in Figure 7, leads to

$$P_{m,loss}(k) = P_{m,loss}(\tau_m(k), \omega_m(k), P_m(k)). \tag{28}$$

Moreover, the EM power dissipation $P_{m,loss}$ is influenced by its size (in torque and speed). In this work, the maximum EM torque ($\bar{\tau}_m$) is scaled down by using the scaling factor s_τ , as shown in Figure 8. The base speed is increased ($\omega_{m,b}^s$) such that the maximum output power is maintained, that is,

$$\bar{P}_m = \bar{\tau}_m \omega_{m,b} = s_\tau \bar{\tau}_m \omega_{m,b}^s. \tag{29}$$

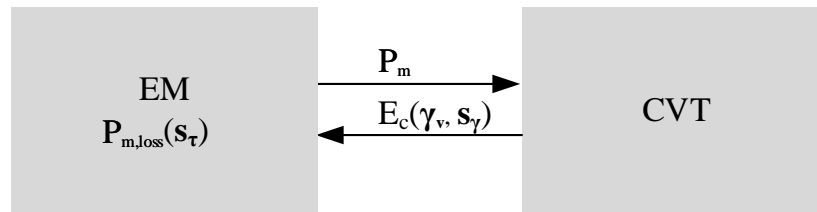


Figure 7. Convex modeling of the EM, where P_m represents the EM output power.

The EM sizing is performed based on the design variable s_τ , because it affects the EM efficiency, weight and cost. For example, reducing the maximum EM torque decreases the usage of active materials of the EM. Note that because of physical limitations of the CVT, the EM speeds above 6500 rpm are not used for the CVT application, which has a negligible impact on the result.

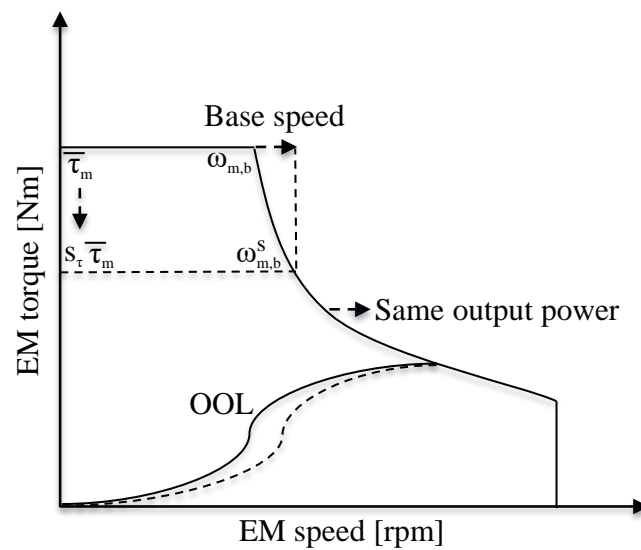


Figure 8. Scaling factor of the EM including the DC-AC inverter, where the solid lines represent the original EM, dashed lines the scaled EM while keeping the same output power, and optimal operating line (OOL) the optimal operating line minimizing the EM losses for every power demand.

The EM scaling factor s_τ influences the EM torque, optimal operating line (OOL) and power losses, which is bounded by

$$s_\tau \in [\underline{s}_\tau, \bar{s}_\tau]. \tag{30}$$

As illustrated in Figure 4b, the scaling of EM has a direct effect on the CVT design requirements. Furthermore, as explained before, the EM power dissipation $P_{m,loss}$ is influenced by another design variable s_γ and control variable γ_v , which change its operating point and hence the power losses. The information of s_γ and γ_v are represented by E_c .

To sum up, the identified parameters that affect the EM power losses are P_m , s_τ , and $E_c(\gamma_v, s_\gamma)$, which are shown in Figure 7. Models that contain these parameters and their combinations, which are also potentially convex, are built. In a similar fashion as with the convex CVT modeling (Section 3.4), the EM models are fitted to capture the loss behavior of the EM. On the basis of fitting accuracy, the convex EM model is found as follows:

$$P_{m,loss}(k) = c_{m,0} \frac{P_m^2(k)}{E_c(k)} + c_{m,1} E_c(k) + c_{m,2} |P_m(k)| + c_{m,3} s_\tau + c_{m,4}, \tag{31}$$

where $c_{m,0}$, $c_{m,1}$, $c_{m,2}$, $c_{m,3}$ and $c_{m,4}$ are the corresponding coefficients. The information of speed and torque are conveyed already by $|P_m|$, and it is further reinforced by torque squared $\frac{P_m^2}{E_c}$ and speed squared E_c to capture essential EM dynamics. Based on Appendix C, this model is convex. It has a fitting accuracy of around 95%. An example of $s_\tau = 1$ is illustrated in Figure 9, where the EM power dissipation is a function of the EM power and $E_c(\gamma_v, s_\gamma)$. A good resemblance can be seen between the developed convex EM model and the original model on the basis of the measurement data. As represented by the absolute error, the difference between them is small. This implies that the developed convex model captures the loss behavior of the EM with sufficient accuracy. Notice that all the EM torque and speed combinations are taken into consideration in constructing the model, and some of them result in higher losses, leading to a larger discrepancy in the upper part of Figure 9. The EM, in practice, however, will not operate at those points. These points are outside the torque-speed envelope, which will be constrained by the EM power limitation model and will be described next. The relatively lower correlation accuracy in the lower part is due to the fact that both motoring and generating modes are considered. Taking into account limited operating points in this part for a long drive cycle in practice, the impact is small.

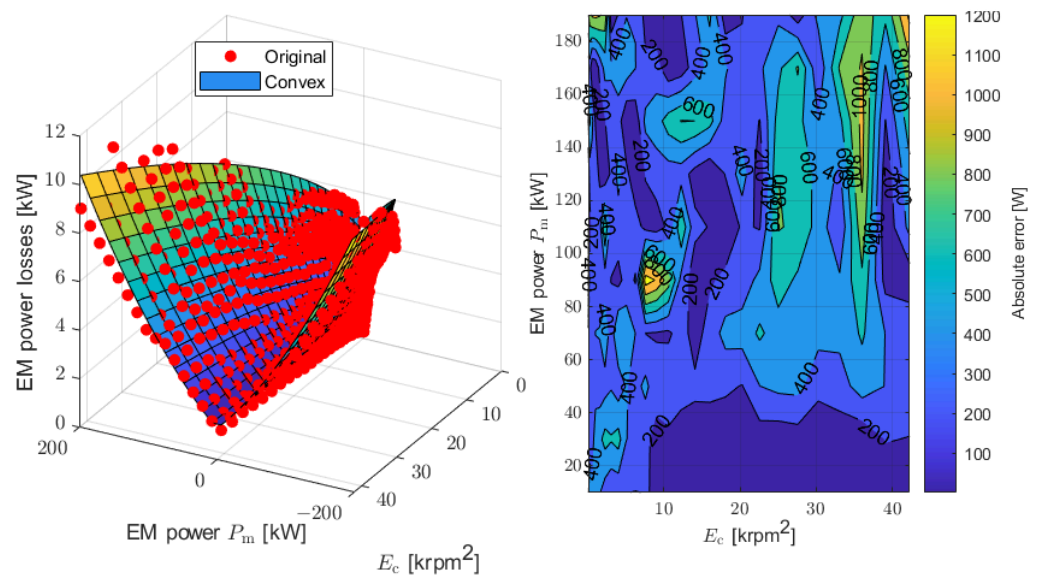


Figure 9. Convex EM power loss model for $s_\tau = 1$. The absolute error represents the difference in power loss between the convex model and the original model based on the measurement data.

3.6. Convex EM Power Limitation Model

As s_τ varies, the EM power limits change as well, referring to (29), as shown in Figure 10. Note that the EM power limits also consider the effect of the CVT ($E_c(\gamma_v, s_\gamma)$). Regarding the EM power limits, as can be seen from Figure 8, they mainly relate to two parts, that is, one before the base speed and the other after the base speed ($\omega_{m,b}$). Hence, the speed information is important. As speed information is mostly conveyed by E_c , it is identified as one of the key parameters. As a result, factors that influence the EM power limits could be, for example, s_τ and $E_c(\gamma_v, s_\gamma)$. Based on these parameters, possible models that preserve convexity are developed, which are fitted to represent the EM power limitation. Based on fitting accuracy, the convex EM power limitation model including motoring and generating modes is identified as follows:

$$\bar{P}_m = \min\{(c_{m,0}^+ E_c(k) + c_{m,1}^+ \sqrt{s_\tau E_c(k)} + c_{m,2}^+ s_\tau + c_{m,3}^+), s_\tau \bar{P}_m\}, \quad (32)$$

$$\underline{P}_m = \max\{(c_{m,0}^- E_c(k) + c_{m,1}^- \sqrt{s_\tau E_c(k)} + c_{m,2}^- s_\tau + c_{m,3}^-), s_\tau \underline{P}_m\}, \quad (33)$$

where $c_{m,0}^+$, $c_{m,1}^+$, $c_{m,2}^+$, $c_{m,3}^+$, $c_{m,0}^-$, $c_{m,1}^-$, $c_{m,2}^-$ and $c_{m,3}^-$ are the corresponding coefficients. The plus sign (+) represents the motoring mode and the minus sign (-) the generating mode. This model is convex (Appendix C) and has a fitting accuracy of around 99%. The terms \bar{P}_m and \underline{P}_m represent the maximum and minimum power of the original EM, respectively, which can be obtained from Figure 8. An example of this model for $s_\tau = 1$ in motoring mode (\bar{P}_m) is depicted in Figure 11, which can be mirrored for generating mode (\underline{P}_m). It can be observed that the developed convex EM power limitation model and the original model based on the measurement data resemble well. It indicates that the developed convex model replicates the power limitation of the EM in reality. It should be noted that while the approximated convex model appears as straight lines in Figure 11 for $s_\tau = 1$, they may not be for other scaling factors, depending on (32) and (33). Notice that, this model is mainly used in Section 4.3.

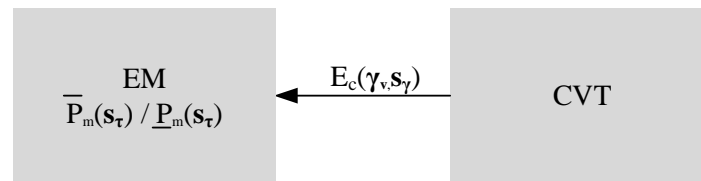


Figure 10. Convex modeling of the EM power limits.

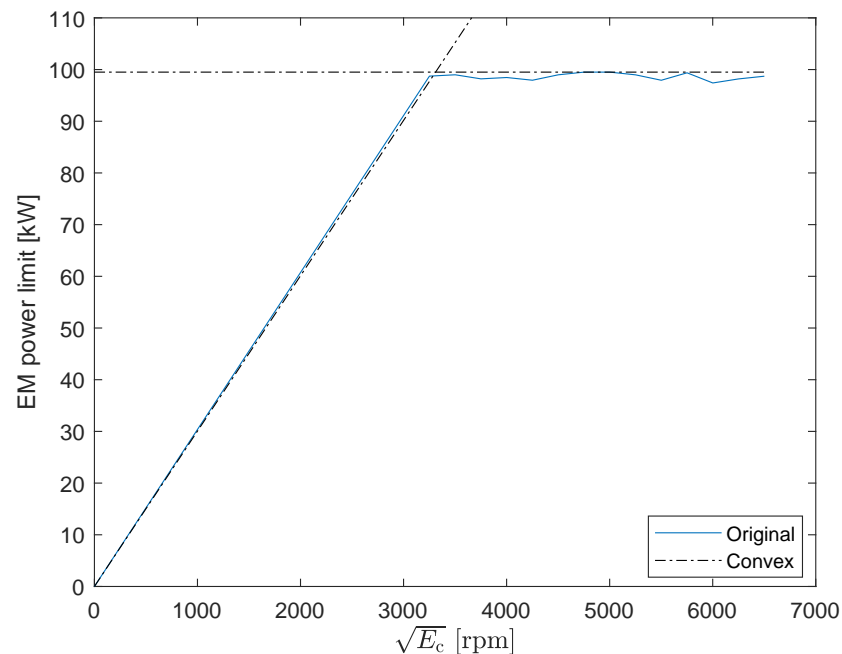


Figure 11. Convex EM power limitation model for $s_\tau = 1$ in motoring mode (\bar{P}_m). The dash-dot lines represent the approximated convex model before and after the base speed.

3.7. Thermal EM-CVT Model

The heat (power losses) generated by the CVT ($P_{c,loss}^s$ in (24)) and EM ($P_{m,loss}$ in (31)) is removed by a TMS, as demonstrated in Figure 12. The main difference between Figures 12 and A4 is that there is an extra small off-the-shelf heat exchanger in Figure 12. It enables heat exchange between the CVT cooling medium and the EM cooling medium. The EM and the CVT are physically attached. The heat from the CVT is removed directly by its cooling medium, which exchanges that with the EM cooling medium. Furthermore, the heat from the EM is taken away by its cooling medium driven by a pump, which is eventually removed by the radiator with a fan providing the required air-flow rate. The EM and CVT dissipate heat to the ambient air due to convection. The aim of the TMS is to find the desired air-flow rate (ϕ_a) that maintains the EM temperature (θ_m) below its prescribed

thermal limit (65 °C) dictated by the manufacturer. A lumped-parameter approach is utilized to describe the thermal behavior of the EM and CVT. Based on first principles of thermodynamics, referring to Appendix A.4, the thermal EM-CVT model is given by

$$c_m m_m \dot{\theta}_m(k) = P_{m,loss}(k) - h_m A_m (\theta_m(k) - \theta_o(k)) - k_m (\theta_m(k) - \theta_c(k)) - h_a A_a (\theta_m(k) - \theta_a), \quad (34)$$

$$c_f m_f \dot{\theta}_o(k) = h_m A_m (\theta_m(k) - \theta_o(k)) - \phi_f c_f (\theta_o(k) - \theta_i(k)), \quad (35)$$

$$c_h m_h \dot{\theta}_h(k) = k_h (\theta_c(k) - \theta_h(k)) - \phi_f c_f (\theta_h(k) - \theta_o(k)), \quad (36)$$

$$c_h c_c m_c \dot{\theta}_c(k) = P_{c,loss}^s(k) + k_e (\theta_m(k) - \theta_c(k)) - k_h (\theta_c(k) - \theta_h(k)) - h_c A_c (\theta_c(k) - \theta_a), \quad (37)$$

$$c_f m_f \dot{\theta}_i(k) = \phi_c c_f (\theta_h(k) - \theta_i(k)) - \epsilon \phi_a(k) c_a (\theta_h(k) - \theta_a). \quad (38)$$

The thermal variables are restricted by

$$\theta_m(k) \in [\underline{\theta}_m, \bar{\theta}_m], \quad (39)$$

$$\theta_o(k) \in [\underline{\theta}_o, \bar{\theta}_o], \quad (40)$$

$$\theta_i(k) \in [\underline{\theta}_i, \bar{\theta}_i]. \quad (41)$$

This model is validated against measurement data in terms of temperature, which is presented in Appendix A.4. Note that since detailed pump and fan signals are not available in the measurement data, validation of cooling power consumption is not performed. Hence, the cooling power consumption is not added to the overall energy consumption. It does not influence the purpose of this study, focusing on evaluation of thermal performance (Section 4.4).

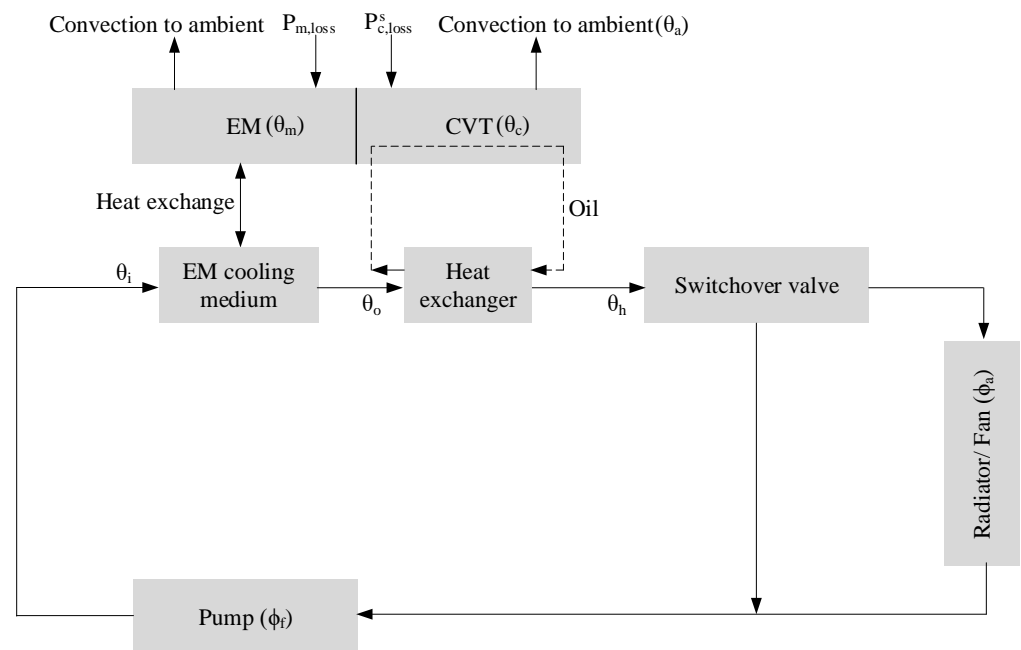


Figure 12. Thermal management configuration for the EM-CVT.

3.8. Convex Battery Model

The electric power of the EM is provided by the battery. The battery model is based on lithium-ion technology with identical cells. The required battery power is given by

$$\begin{aligned} P_b(k) &= P_{el}(k) + P_{b,loss}(k) \\ &= P_m(k) + P_{m,loss}(k) + P_{b,loss}(k), \end{aligned} \quad (42)$$

where $P_{b,\text{loss}}$ represents the battery losses, which is calculated by

$$\begin{aligned} P_{b,\text{loss}}(k) &= s_b N_0 I_c^2(k) R_c \\ &= \frac{P_b^2(k) R_c}{s_b N_0 V_c^2(k)}, \end{aligned} \quad (43)$$

where I_c is the cell current and R_c its resistance. The battery sizing is performed based on the scaling factor s_b for scaling the battery cells, which linearly influences the battery energy, weight and cost. N_0 is the original number of battery cells when $s_b = 1$. To preserve convexity for the co-design problem (Appendix C), the open circuit voltage of a battery cell (V_c) is approximated as a linear function of the state-of-charge of the battery (ξ), given by

$$V_c(k) = \frac{Q_c}{F_c} \xi(k) + V_0, \quad (44)$$

where Q_c is the cell capacity and F_c the capacitance. The battery energy can then be calculated by

$$\begin{aligned} E_b(k) &= s_b N_0 \int_0^{\xi} V_c(k) Q_c d\xi \\ &= \frac{F_c}{2} s_b N_0 (V_c^2(k) - V_0^2). \end{aligned} \quad (45)$$

Taking the derivative of E_b yields

$$\dot{E}_b(k) = -P_b(k). \quad (46)$$

In order to model the battery on a pack level instead of a cell level, which does not require information of series-parallel connection, the cell voltage V_c is replaced by a new variable U_b , by applying a change of variables, given by

$$U_b(k) = s_b N_0 V_c^2(k) = \frac{2}{F_c} E_b(k) + s_b N_0 V_0^2. \quad (47)$$

The battery power losses can then be expressed as

$$\begin{aligned} P_{b,\text{loss}}(k) &= \frac{P_b^2(k) R_c}{U_b(k)} \\ &= \frac{P_b^2(k) R_c F_c}{2 E_b(k) + s_b N_0 F_c V_0^2}. \end{aligned} \quad (48)$$

The battery energy and power are constrained by

$$E_b(k) \in \left[\frac{F_b}{2} s_b N_0 (V_c^2 - V_0^2), \frac{F_b}{2} s_b N_0 (\bar{V}_c^2 - V_0^2) \right], \quad (49)$$

$$P_b(k) \in [I_c V_b(k), \bar{I}_c V_b(k)], \quad (50)$$

where V_b is given by

$$\begin{aligned} V_b(k) &= s_b N_0 V_c(k) \\ &= \sqrt{s_b N_0 U_b(k)}. \end{aligned} \quad (51)$$

3.9. Convex Mass and Cost Models

Apart from powertrain and thermal models, convex mass and cost models are required for the implementation of the co-design method. This section describes the convex mass

and cost models associated with the CVT, EM and battery sizes. The CVT mass includes the mass of the variator and final drive. The EM mass includes the mass of the EM and inverter.

For a generic CVT, its weight can be approximated as a function of its torque capacity $\bar{\tau}_c$ based on existing CVTs [25]. The CVT weight m_c is modeled by

$$m_c = 0.28 \bar{\tau}_c + 23.21. \quad (52)$$

The original production CVT with a full ratio range of [0.38, 2.63], implying a ratio coverage of around 7, has a torque capacity of 250 Nm. On the basis of this CVT, assume the ratio affects the torque capacity proportionally. For each torque capacity (ratio coverage), the corresponding weight can be computed based on (52). Specifically for the CVT in this study, a one-on-one mapping between the weight m_c and ratio coverage s_γ can thus be expressed as

$$m_c = 1.19 s_\gamma^2 + 39.12. \quad (53)$$

Therefore, given the specific cost of CVT [23] (a_c in Table A1), the CVT cost C_c (in €) is given by

$$C_c = a_c (1.19 s_\gamma^2 + 39.12). \quad (54)$$

The prediction (54) is valid on the basis of this CVT, since the ratio coverage is scaled down.

The EM weight is estimated as a function of its scaling factor [26], that is,

$$m_m = s_\tau \bar{m}_m, \quad (55)$$

where \bar{m}_m is the original EM mass when $s_\tau = 1$, which is provided in Table 1.

The EM cost C_m (in €) is estimated as a function of its scaling factor [27,28], giving

$$C_m = b_m s_\tau. \quad (56)$$

The battery weight is described as a function of its scaling factor, given by

$$m_b = s_b \bar{m}_b, \quad (57)$$

where \bar{m}_b is the original battery mass when $s_b = 1$, which is provided in Table 1. The battery cost C_b (in €) is approximated by [28,29]

$$C_b = s_b c_b \bar{E}_b. \quad (58)$$

Note that, the price of CVT could be lowered, as some parts of the CVT for conventional applications are not needed in EVs, such as torque converter and DNR (drive, neutral and reverse). However, since part of this information is taken into account in (53) and the exact weight is not known before optimization, it is not further addressed. Moreover, currently, there is no consensus on the component price. The numbers used in this study are only indicative figures (e.g., $b_m, c_b \bar{E}_b$), which have no direct relation to possible market prices. They do not affect the comparison, as the same scale is employed in all the systems (S_1, S_2 and S_3).

Additionally, notice that the component specifications appear large in this case. The components are scaled down, which means that, for example, $s_\tau > 1$ and $\gamma_v > 2.63$, are not necessary. The models are always valid within their feasible ranges based on the measurement data. The right combination of the speed ratio of the CVT over time γ_v , air-flow rate of the cooling system ϕ_a , ratio coverage s_γ , the scaling factor for the EM s_τ and the scaling factor for the battery s_b will be determined simultaneously by the optimization algorithm, which is discussed in the next section.

This section presents a convex EV model and its associated cost models for the co-design optimization problem. A data-driven approach is used to derive the convex CVT and EM models. In particular, the coupling between the EM and CVT from design and

control perspectives is described in detail. Compared to the original model based on measurements, the convex CVT power loss model is developed with a correlation accuracy of 98%. The convex EM power loss and power limitation models are developed with correlation accuracies of 95% and 99%, respectively. An experimentally validated thermal EM-CVT model is subsequently presented. A convex battery model is also developed. Finally, convex mass and cost models that are size-dependent for the CVT, EM and battery are created. The overall system has a large number of states, and there is a strong coupling between the CVT and EM. By applying CP, not only will it find an optimal solution but also it will find the solution in a computationally efficient manner. It allows for extensive parameter variation studies and evaluation of diverse design aspects on system and component level.

4. Optimization Results and Discussion

On the basis of the convex models developed in the last section, the objective of the co-design optimization strategy is to minimize the TCO. It aims at generating an optimal control trajectory of the speed ratio of the CVT (γ_v) and finding the desired air-flow rate of the cooling system (ϕ_a). Furthermore, it aims to identify the optimal sizes of the CVT (s_γ), EM (s_τ) and battery (s_b). Based on (1), the overall co-design optimization problem in S_3 can be written as follows:

$$\begin{aligned} \min \sum_{k=1}^N \rho_e P_b(s_\gamma, s_\tau, s_b, E_b(k), \theta_m(k), \theta_c(k), \theta_o(k), \theta_i(k), \phi_a(k), \gamma_v(k) \mid v_v(k), a_v(k)) \Delta t \\ + \frac{S_d}{S_v} (C_c(s_\gamma) + C_m(s_\tau) + C_b(s_b)), \end{aligned} \quad (59)$$

$$\text{s.t. (11) – (58).} \quad (60)$$

The final state of the battery energy is not constrained, considering the battery capacity and the power demand of the drive cycle. The overall optimization problem is convex, including convex cost function, models and constraints. Basic convex functions, for example, linear, quadratic, quadratic-over-linear and opposite of geometric mean functions, and operations that preserve convexity, for example, nonnegative weighted sums and pointwise maximum, are used to verify model convexity. For example, the battery mass model (57) is linear and the CVT cost model (54) is quadratic. A quadratic-over-linear term is used in the EM loss model (31). The overall co-design optimization problem is solved by using SDPT3 [30]. Specifically, the problem can be recognized as a semidefinite program. It is then translated automatically by a tool CVX into a form required by SDPT3 [30]. This permits the problem to be written in a readable form, for example, using expressions/symbols to hold operations over variables. It solves the dual problem for improved efficiency [22].

4.1. Control and Design Freedom

The co-design optimization method tends to obtain a globally optimal solution by simultaneously optimizing the design and control variables to minimize the TCO. Figure 13 shows the EM operating points on the WLTC for the three systems. It can be seen from Figure 13 that the EM operation in S_1 is relatively fixed, which has no control freedom because of the fixed gear ratio (9.02 in Table 1). The EM has to operate according to the driving conditions, which can hardly be efficient in consideration of real-world dynamic behavior. In contrast, the EM in S_2 has relatively more freedom to adjust operating points to reduce the power dissipation. This is realized by changing the speed ratio of the CVT, depending on the loading conditions. Yet, implementing the standard CVT controllers developed for conventional vehicles would reduce only the EM power losses (Section 2), regardless of the CVT efficiency. While the EM operation in S_2 is efficient, which follows its OOL (Figure 13), the system (combined EM and CVT) is not able to operate efficiently over a dynamic cycle (WLTC). The combined EM and transmission losses are thus higher in S_2 than that in S_1 , as shown in Figure 14. The co-design optimization strategy, however, takes full advantage of control freedom (continuous ratio adjustment depending on the

driving conditions) provided by the CVT. Specifically, apart from the EM power dissipation, the CVT power losses are also monitored in S_3 . The CVT speed ratio over time γ_V (19) is selected to improve the overall system efficiency. Ratio variation that results in a higher loss is penalized. Smooth ratio change improves efficiency, drivability and reduced ELOP power losses. This effect can be seen in Figure 14, where the CVT power dissipation in S_3 is significantly lower than that in S_2 and the system efficiency is higher. The EM efficiency is also high in S_3 , as demonstrated in Figure 13. The battery power dissipation is similar in three systems.

Additionally, the control freedom offered by the CVT creates design flexibility, which is not explored by S_2 , as the component sizes are fixed. The design space is larger in S_3 , with different combinations of CVT (21) and EM (30) sizes, which bring opportunities of optimizing the system from design perspective. The optimal component sizes, namely the right combination of the scaling factor for the battery (s_b^0), scaling factor for the EM (s_t^0) and the ratio coverage of the CVT (s_γ), are eventually determined by the co-design optimization method. The co-design optimization strategy takes into account the coupling between the EM and CVT, cost function and the drive cycle.

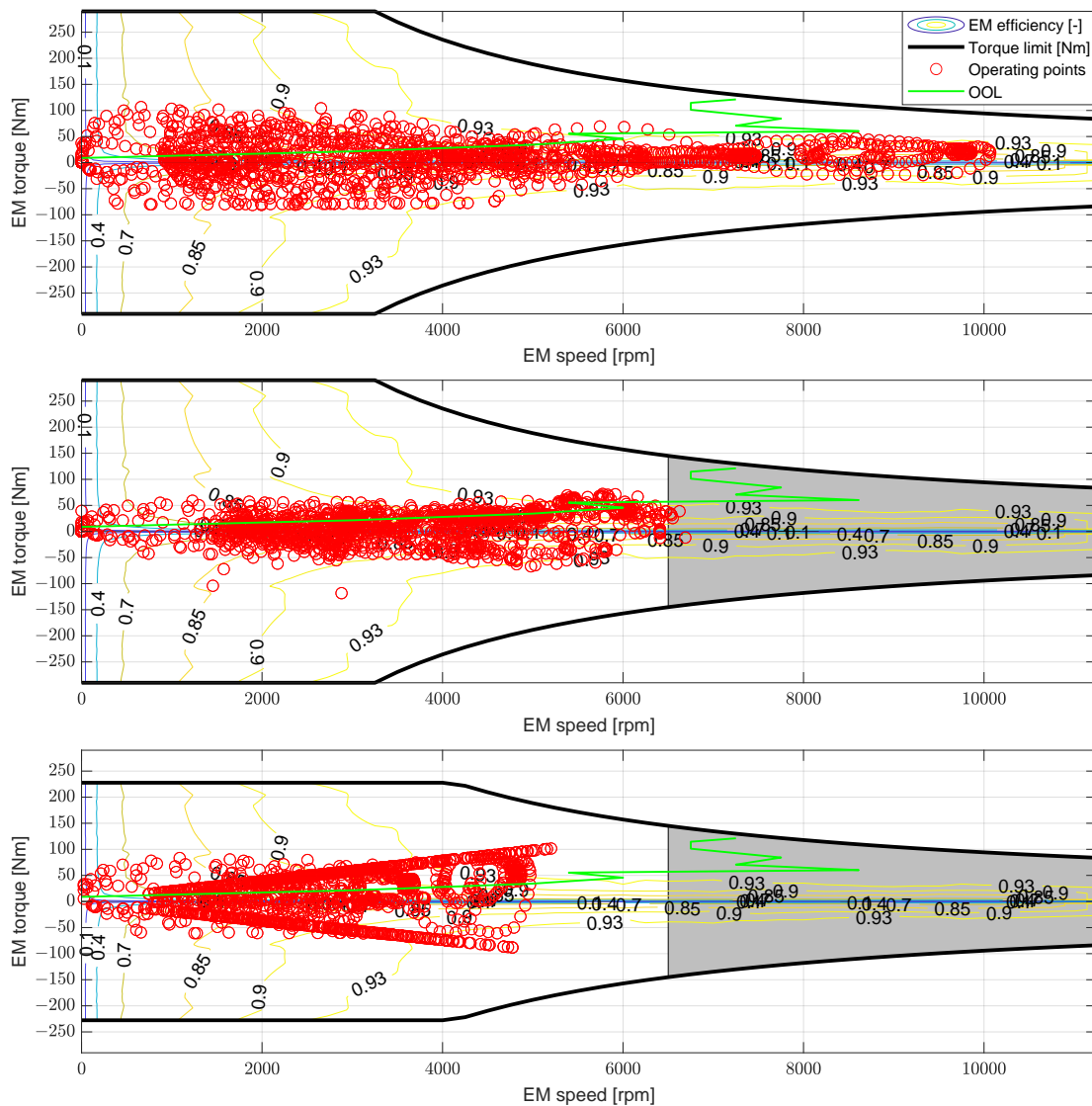


Figure 13. EM operating points on the Worldwide Harmonized Light Vehicles Test Cycles (WLTC). (Top to bottom) S_1 , S_2 , and S_3 .

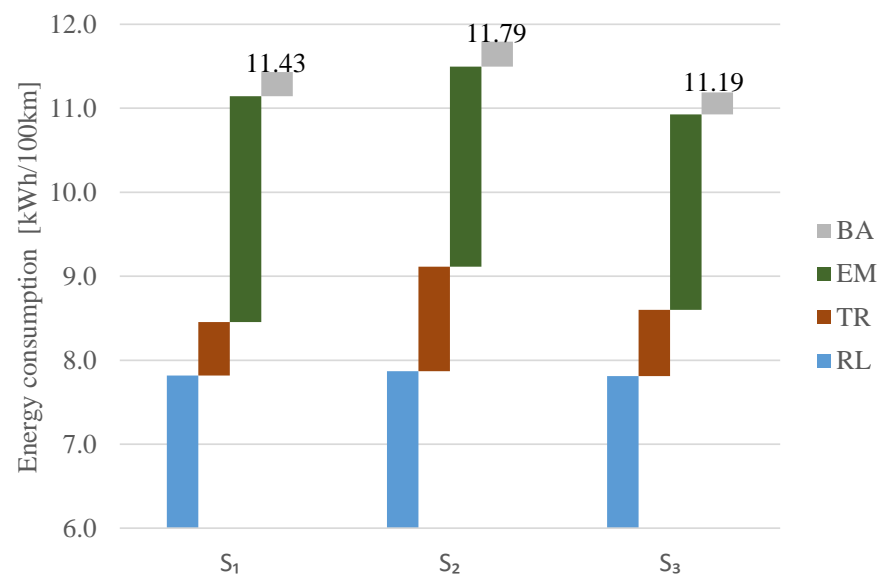


Figure 14. Comparison of energy consumption between S_1 (with a total vehicle mass of 1670 kg), S_2 (with a total vehicle mass of 1700 kg) and S_3 (with a total vehicle mass of 1666 kg) on the WLTC, where RL represents road load. The transmission (TR) losses include the ELOP power dissipation, which is zero in S_1 . The EM power losses include the effect of the DC-AC inverter.

As shown in Table 1, the maximum EM torque is reduced from $s_\tau = 1$ in S_1 and S_2 to $s_\tau = 0.79$ in S_3 . Reduced EM torque and increased base speed decrease the EM losses (Figure 13). The optimal battery size is found and the number of battery cells is reduced because of improved efficiency (Table 1). The EM in S_3 has the same maximum power as the other systems. Because the same EM from the SST-based EV on the market (S_1) is utilized in S_2 , which is not optimized for the CVT application. Even if the EM is made smaller in S_2 , the overall system efficiency is not necessarily always be higher, see Figure 8 about the OOL, as the CVT efficiency is not considered.

This reduced EM size is achieved due to a variable ratio coverage. The right ratio coverage of the CVT can also thus be determined in combination with the EM size in terms of torque and power. It is reduced from [0.7, 2.63] with a ratio coverage of 3.76 before optimization to [0.7, 2.34] with a ratio coverage of 3.34 after optimization (Table 1). In S_2 , the CVT is oversized considering the WLTC. First, the CVT used in S_2 is based on an off-the-shelf component, which is not optimized. Second, the CVT is controlled only to reduce the EM power dissipation, regardless of the CVT size. The system mass including transmission, EM and battery (Table 1) is thus reduced in S_3 due to the reduced component sizes, resulting in a decrease in power demand (RL in Figure 14). The curb weight and driver mass are the same in the three systems.

Owing to high CVT power losses in S_2 , the energy consumption is reduced by around 3.1% in S_1 . Compared with S_2 , because of the reduction in the system power losses (Figure 14), the energy consumption is decreased by around 5.1% in S_3 . The decrease in the CVT power dissipation contributes more to the energy saving. Given the component sizes, the component costs are calculated based on (54), (56) and (58). As shown in Figure 15, compared with S_1 , the system cost is increased by around 5.1% in S_2 , as the CVT cost is higher than the SST price. Due to the reduction in the component sizes (Table 1), compared to S_1 , the system cost is reduced by around 1.8% in S_3 . Reduced EM torque decreases the EM mass and cost. The decrease in the battery and EM prices contributes more to the cost saving.

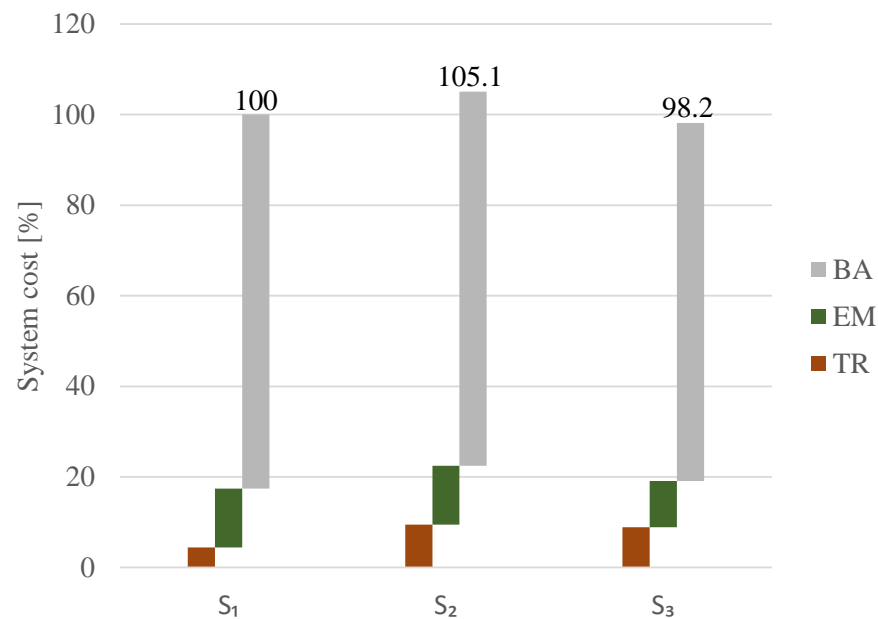


Figure 15. Comparison of normalized system cost between S_1 , S_2 and S_3 , where the EM cost includes the DC-AC inverter.

Overall, as shown in Figure 16, S_3 has the lowest TCO because of reduced energy consumption and system cost, which is around 2% lower than S_1 . The optimization results demonstrate that the optimized EM-CVT system can be compact, lightweight, energy-efficient and cost-effective. It is very different from its traditional image. Additionally, it can be suggested that automotive suppliers could greatly benefit from highly integrated components and systems to maximize their system efficiency and minimize cost targets. It can also be observed that reducing the maximum EM torque and increasing the base speed while having a higher slope of OOL compared with that of SST are beneficial for CVT-based EVs (Figure 13). Most importantly, it shows the importance of cycle-driven (Section 3.2) and co-design (Section 2) in identifying the optimal control trajectories and component sizes. Specifically, it finds the trade-off between CVT power losses (24), CVT size (21), EM power losses (31), and EM size (30), based on the combined EM-CVT characteristics (Figure 7) and cost function (1).

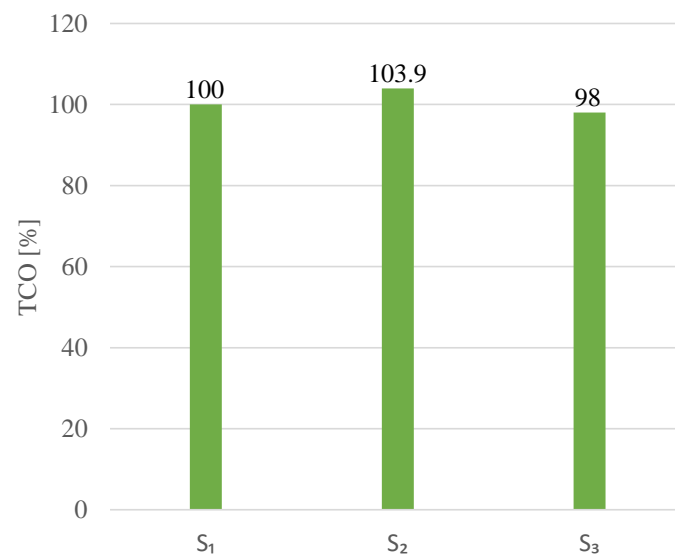


Figure 16. Comparison of normalized TCO between S_1 , S_2 and S_3 .

4.2. Sequential Design versus Simultaneous Design

The strength of co-design (simultaneous design in this case) lies in the fact that it finds the optimal design and control variables simultaneously. It minimizes the cost function for a strongly coupled problem, which is the case for the integration of the EM and CVT (Figure 1). The CVT speed ratio (control) influences the CVT and EM sizes (design/plant), and vice versa (e.g., (24) and (31)). The cost function, namely the minimization of the TCO (1), consists of the energy consumption (9) and system cost (10), and both are affected by the design and control variables. In order to demonstrate the effectiveness of the co-design approach in S_3 , it is compared to a sequential design (SD) method, where the plant and controller are determined sequentially (Section 1). Note that for purposes of comparison, not all the plant parameters are predetermined. SD is defined as follows:

- SD: Based on S_3 , assuming that the EM size is fixed (i.e., $s_\tau = 1$) in order to achieve the required performance (Section 1), the goal is to find the CVT speed ratio over time, CVT and battery size reducing the TCO.

Referring to (1), the corresponding cost function is given by

$$\min \sum_{k=1}^N \rho_e P_b(s_\gamma, s_b, x(k), u(k) | s_\tau) \Delta t + \frac{S_d}{S_v} (C_c(s_\gamma) + C_m + C_b(s_b)), \quad (61)$$

where C_m is a constant because of the fixed EM size. Other constraints remain the same. The comparison between SD and S_3 is shown in Figure 17.

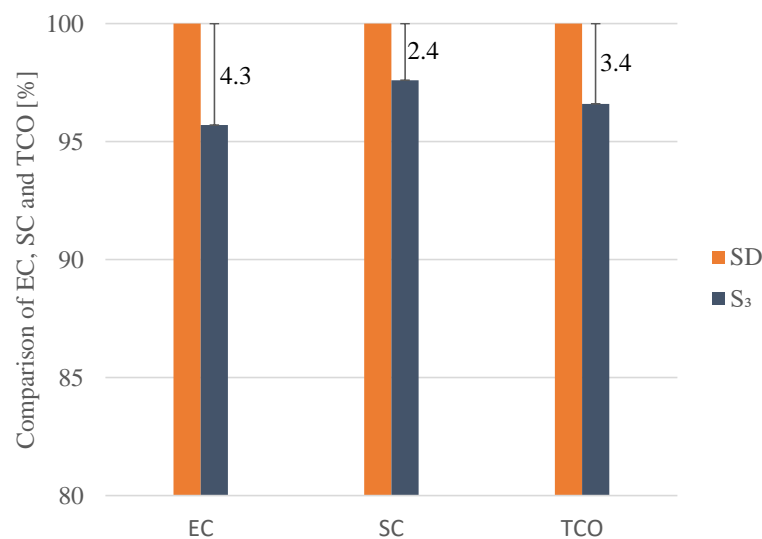


Figure 17. Comparison of normalized EC, SC and TCO between SD (with a total vehicle mass of 1677 kg) and S_3 , where EC represents the energy consumption and SC the system cost.

It can be seen from Figure 17 that the energy consumption (EC) and system cost (SC) are reduced in S_3 compared with SD. Overall, the TCO is decreased by around 3.4% in S_3 . The primary reason is that the control and design freedom provided by the CVT cannot be fully exploited in SD because of the fixed EM size. Admittedly, the CVT is optimized in SD, especially the CVT cost because of a reduced ratio coverage of around 2, which is significantly lower than that of 3.34 in S_3 . Nevertheless, the EM and battery optimization are not taken into account, leading to a higher system cost. The control trajectory identified may not be efficient for the overall system. In SD, the problem is decoupled and the interconnections between the CVT (24), EM (31) and battery (42) are not considered, resulting in a higher TCO. For an inherently coupled problem (i.e., the integration of the EM and CVT), SD creates a separation and cannot guarantee an optimal solution. This issue is tackled by the co-design approach (S_3), where the right combination of the control policy

and component sizes reducing the TCO is identified. It considers the coupling between the components from design and control perspectives.

4.3. Towards a Low-Power Application

As illustrated in Figure 13, the usage of the available EM torque is low considering WLTC. It implies that powertrain components are typically oversized (considering WLTC) to meet certain vehicle performance requirements. The selection of electric powertrain components (e.g., EM) for future EV applications is still an ongoing question. Current selection criteria are largely based on performance requirements, such as top speed, acceleration time and gradability (Section 1). It usually leads to oversized components, considering drive cycles used for efficiency indicators. Therefore, even with the co-design approach, the downsizing potential is limited (Section 4.1). High performance, however, may not be required in urban driving. In order to see the downsizing potential, a low-power (LP) design is utilized as an example. Note that for purposes of comparison, the EM design is not restricted by (29). LP is defined as follows:

- LP: Based on S_3 , assuming that there are no performance requirements (Section 1), the aim is to find the optimal design and control variables reducing the TCO while satisfying drive cycle requirements.

The objective function in this case is similar to (1). The comparison between LP and S_3 is shown in Figure 18. It can be observed from Figure 18 that compared with S_3 , the energy consumption (EC) and system cost (SC) are decreased in LP. Overall, in LP, the TCO is reduced by around 4%. The main reason is that LP takes full advantage of the control and design freedom provided by the CVT without performance constraints. Compared to S_3 , all the parameters as presented in Table 1, Figures 14 and 15 are reduced in LP. For example, the maximum EM power is reduced from 100 kW in S_3 to 54 kW in LP with a CVT ratio coverage of around 2.06. The battery size is decreased in LP as well. The minimum required component size is found in LP. For a specific use case (WLTC) and a given EM-CVT system (combined EM-CVT characteristics), there is a lower bound for the system (i.e., the CVT, EM and battery) so as to complete the driving mission. The result also demonstrates the importance of co-design optimization in determining the system size for a representative use case, considering the coupling between the EM and CVT (combined EM-CVT characteristics). Although reduction of peak power has a negative effect on vehicle performance (e.g., the 0–50 km/h and 0–100 km/h acceleration times of LP are around 6 s and 18 s, respectively), LP is energy-efficient and cost-effective. It can be used for urban driving that does not require high performance.

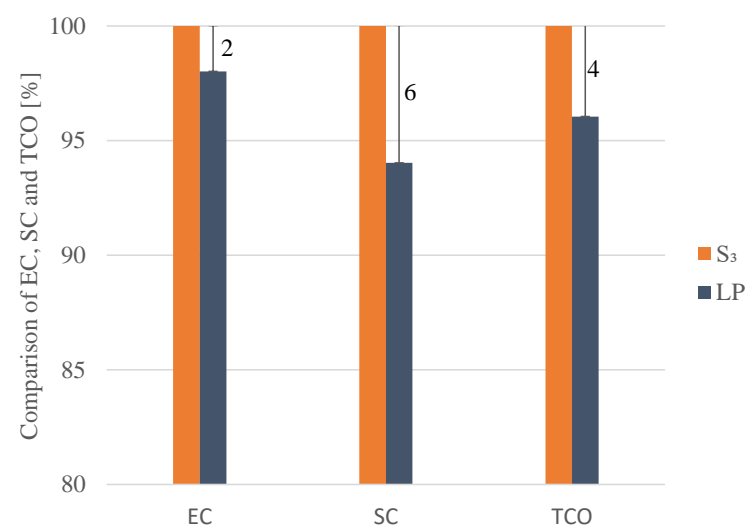


Figure 18. Comparison of normalized EC, SC and TCO between LP (with a total vehicle mass of 1635 kg) and S_3 , where EC represents the energy consumption and SC the system cost.

4.4. Thermal Performance

The EM is a power source. It is also a heat source, and so does the transmission. They generate heat during operation, which needs to be taken away efficiently by a cooling system. For purposes of comparison, S_1 , S_2 and S_3 have the same control target, maintaining the EM temperature below its thermal limit $65\text{ }^\circ\text{C}$ dictated by the manufacturer at the end of the drive cycle. All the other conditions are the same, including the coolant flow rate. For simplicity, the problem is translated to finding a constant air-flow rate for each system over the WLTC. Assume the air-flow rate is proportional to the cooling power consumption. They are compared in terms of cooling power consumption and temperature profile.

It is found that $\phi_a(S_2) = 0.89 \phi_a(S_1)$, which means that compared to S_1 , the cooling power consumption is reduced in S_2 , as shown in Figure 19. Recall that the system losses are higher in S_2 (Figure 14). The EM power dissipation in S_2 is less than that in S_1 but the transmission power dissipation is much higher. In this case, the EM is more dominant in determining the level of the cooling power consumption. Another reason is that the thermal mass (EM and CVT) is higher in S_2 (Table 1). Moreover, because of topology difference, the extra small off-the-shelf heat exchanger in S_2 enables heat exchange between the EM and CVT. It changes the overall thermal behavior of the cooling system. It is also calculated that $\phi_a(S_3) = 0.78 \phi_a(S_2)$, which implies that compared to S_2 , the cooling power consumption is decreased in S_3 . They have the same topology. The primary reason is that the power losses are less in S_3 , which requires less cooling power to remove the heat, although the system mass is reduced in S_3 . The corresponding temperature profiles are illustrated in Figure 20.

Additionally, an important finding from Figure 20 is that the EM temperature and the CVT temperature are very similar in S_3 . The primary reason is that the small heat exchanger provides extra heat exchange between the EM and the CVT. It is a crucial step towards a thermally integrated EM and CVT, for example, using a combined cooling loop with a dedicated cooling medium, taking into account such as corrosion, viscosity and conductivity [31–33]. It would make the system even more compact and efficient.

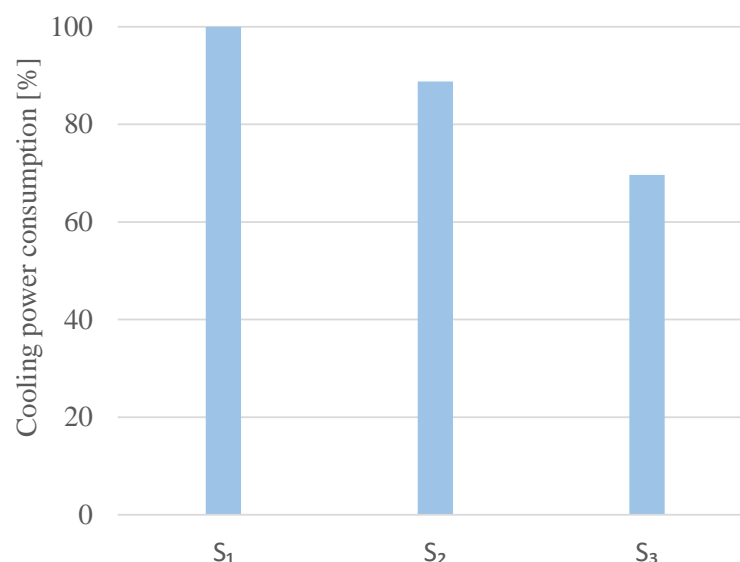


Figure 19. Comparison of normalized cooling power consumption between S_1 , S_2 and S_3 .

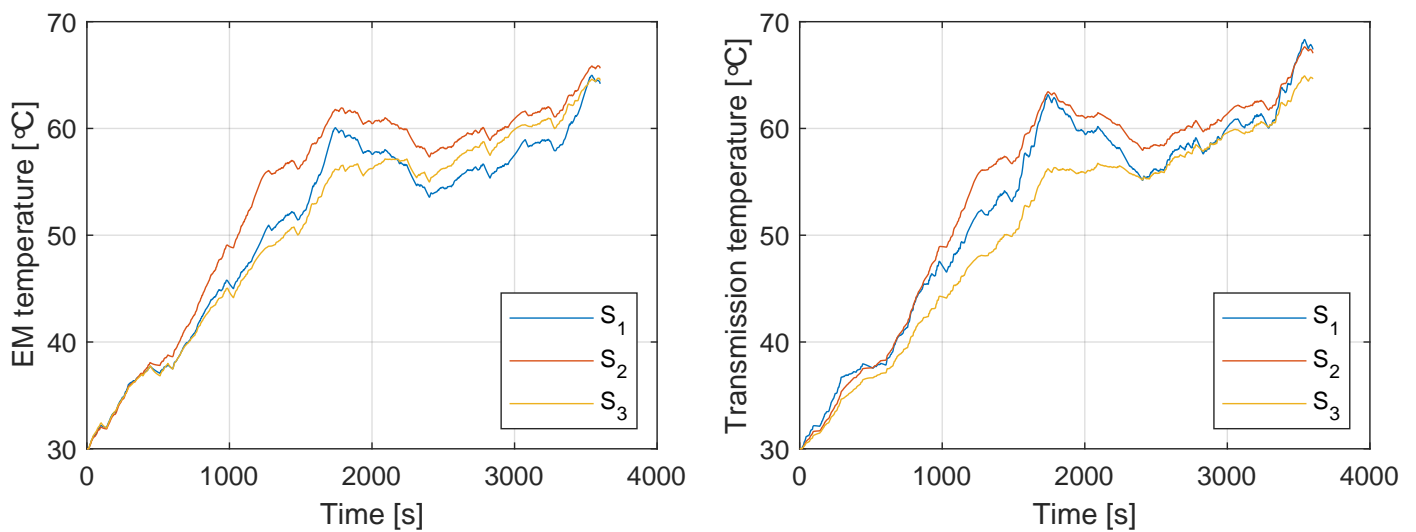


Figure 20. Comparison of temperature profile between S_1 , S_2 and S_3 .

Note that as the systems, overall, are efficient, this amount of reduction will not significantly influence the total energy consumption, although depending on the use case. Furthermore, the exact value of cooling power is not provided, because detailed pump and fan signals are not available in the controller area network (CAN) data, as mentioned in Section 3.7. However, based on physics and model validation (Appendix A.4), the result is representative. Previously, it is shown that there is a strong coupling between the EM and CVT, and the combined system can be lightweight, efficient and low-cost. Now, it is demonstrated that they can also be integrated thermally, and a further reduction in weight, energy usage and cost can be expected. In the future, a highly integrated EM-CVT system can be anticipated for EV applications.

5. Conclusions

A co-design optimization method based on CP is proposed for a CVT-based EV to minimize the TCO, focusing on the integration of the EM and CVT. The co-design optimization method finds the optimal CVT speed ratio, air-flow rate of the cooling system, CVT size, EM size and battery size simultaneously. It takes full advantage of the control and design freedom provided by the CVT. The optimized system with the co-design approach decreases the TCO by around 2% compared with an SST-based EV with reference to a series production vehicle and by around 5.9% compared with a non-optimized CVT-based EV (based on off-the-shelf components). The advantages of the co-design approach are also highlighted by comparing to a sequential method. Moreover, for urban driving, insights into the design of a low-power EV are given based on the co-design approach, which finds the minimum required component size. It can be concluded that although the current EV market is dominated by SSTs, multi-speed transmissions, for example, CVTs, are competitive alternatives for EVs in terms of TCO, due to continuous ratio adjustment depending on driving conditions and the resulting design freedom. For EV applications, a highly and thermally integrated EM-CVT system, which is low-cost, efficient and lightweight, can be anticipated.

Author Contributions: C.W. proposed the concepts and methodologies. He wrote and edited the original draft; T.H. and E.I.C. were responsible for supervision, internal review and editing of the draft and concepts. All authors have read and agreed to the published version of the manuscript.

Funding: This research received no external funding.

Institutional Review Board Statement: Not applicable.

Informed Consent Statement: Not applicable.

Data Availability Statement: No new data were created or analyzed in this study. Data sharing is not applicable to this article.

Acknowledgments: This research was carried out under project number T18001 in the framework of the Research Program of the Materials innovation institute (M2i) (www.m2i.nl accessed on 11 February 2021) supported by the Dutch government.

Conflicts of Interest: The authors declare no conflict of interest.

Abbreviations

The following abbreviations are used in this manuscript:

AC	Alternating Current
BA	Battery
CAN	Controller Area Network
CP	Convex Programming
CVT	Continuously Variable Transmission
DC	Direct Current
DNR	Drive, Neutral and Reverse
DP	Dynamic Programming
EC	Energy Consumption
ELOP	Electric Oil Pump
EM	Electric Machine
EV	Electric Vehicle
FD	Final Drive
ICDC	Intercity Drive Cycle
KPI	Key Performance Indicator
LP	Low Power
OOL	Optimal Operating Line
PSO	Particle Swarm Optimization
RL	Road Load
SC	System Cost
SD	Sequential Design
SST	Single Speed Transmission
TCO	Total Cost of Ownership
TMS	Thermal Management System
TR	Transmission
VA	Variator
VCU	Vehicle Control Unit
WH	Wheel
WLTC	Worldwide Harmonized Light Vehicles Test Cycle

Appendix A. SST-Based EV Model

The SST-based EV model (S_1) is validated by measurement data obtained from the series production vehicle driven on a real-world drive cycle, namely intercity drive cycle (ICDC). The measurement data are extracted from the CAN signals of the vehicle control unit (VCU) in the series production vehicle driven on the ICDC. The sampling time is 0.01 s. The vehicle specification is provided in Table A1.

Appendix A.1. Longitudinal Dynamics

Given the drive cycle represented by vehicle velocity v_v and acceleration a_v and taking into account aerodynamic drag force, rolling resistance and inertia force, the demanded wheel torque τ_w and speed w_w can be calculated by

$$\tau_w(k) = \left(\frac{1}{2} \rho_a c_d A_f v_v^2(k) + c_r m_v g \operatorname{sign}(v_v(k)) + \left(m_v + 4 \frac{J_w}{r_w^2} \right) a_v(k) \right) r_w, \quad (A1)$$

$$\omega_w(k) = \frac{v_v(k)}{r_w}, \quad (\text{A2})$$

where the total vehicle mass m_v is given by

$$m_v = m_{cw} + m_s + \bar{m}_m + \bar{m}_b + m_d, \quad (\text{A3})$$

where m_s is the SST mass (Table 1).

Table A1. Main parameters of EV model.

Parameter	Value	Unit	Description
ρ_a	1.18	kg/m ³	Density of air
c_d	0.27	-	Aerodynamic drag coefficient
A_f	2.21	m ²	Frontal area
c_r	0.00724	-	Rolling resistance coefficient
J_w	1	kgm ²	Wheel inertia
r_w	0.312	m	Wheel radius
η_g	0.98	-	Fixed gear efficiency
η_f	0.985	-	Final drive efficiency
$\bar{\gamma}_v$	2.63	-	Underdrive ratio
$\underline{\gamma}_v$	0.7	-	Overdrive ratio
c_m	430 [19]	J/kgK	Specific heat capacity of EM
c_c	630 [23]	J/kgK	Specific heat capacity of CVT
c_s	630 [23]	J/kgK	Specific heat capacity of SST
c_f	4090	J/kgK	Specific heat capacity of EM cooling medium
c_a	1000	J/kgK	Specific heat capacity of air
c_h	0.62 [23]	-	CVT heating coefficient
h_m	2000	W/m ² K	Heat transfer coefficient between EM and its cooling medium
h_a	10	W/m ² K	Heat transfer coefficient between EM and ambient air
h_c	10	W/m ² K	Heat transfer coefficient between CVT and ambient air
k_m	111	W/K	Heat transfer coefficient between EM and CVT
k_h	125	W/K	Heat transfer coefficient between EM cooling medium and CVT oil
A_m	0.2	m ²	Heat exchange area between EM and its cooling medium
A_a	0.32	m ²	Heat exchange area between EM and ambient air
A_c	0.17	m ²	Heat exchange area between CVT and ambient air
m_f	1.5	kg	Cooling medium mass
ϕ_f	0.35	kg/s	Coolant flow rate
ϵ	0.6 [34]	-	Radiator effectiveness
$\bar{\theta}_m$	65	°C	Maximum EM temperature
$\bar{\theta}_o$	65	°C	Maximum cooling medium temperature at EM outlet
$\bar{\theta}_i$	65	°C	Maximum cooling medium temperature at EM inlet
S_d	46.532	km	Two repeated WLTC length
S_v	300,000	km	Traveled distance of vehicle in its lifetime
ρ_e	0.23	€/kWh	Price of electricity
a_c	13 [23]	€/kg	Specific cost of CVT
b_m	1000	€	Specific cost of EM
c_b	250	€/kWh	Specific cost of battery
\bar{E}_b	25.4	kWh	Battery energy
N_0	264	-	Battery cells

Appendix A.2. Single-Speed Transmission

The SST including the final drive provides a fixed speed ratio γ_s between the EM and the wheel. To meet the torque and speed at the wheels given by (A1) and (A2), the required torque and speed of the SST are obtained by

$$\tau_s(k) = \begin{cases} \frac{\tau_w(k)}{\eta_s \gamma_s}, & \text{if } \tau_w(k) > 0, \\ \frac{\eta_s \tau_w(k)}{\gamma_s}, & \text{if } \tau_w(k) \leq 0, \end{cases} \quad (\text{A4})$$

$$\omega_s(k) = \gamma_s \omega_w(k), \quad (\text{A5})$$

where η_s is the combined efficiency of the fixed gear η_g and the final drive η_f (Table A1).

Appendix A.3. Electric Machine

The EM is a permanent magnet synchronous machine, featuring motoring and generating modes. Its specification is provided in Table 1. The torque and speed of the EM are computed by

$$\tau_m(k) = \tau_s(k), \quad (\text{A6})$$

$$\omega_m(k) = \omega_s(k). \quad (\text{A7})$$

Given the same inputs (vehicle speed and acceleration) from the ICDC, the outputs of the EM from the developed model (simulation) are compared with the corresponding CAN signals (measurement). These signals are the EM torque and speed, and the comparisons are shown in Figures A1 and A2, respectively. In Figures A1 and A2, the right subplot zooms in on the left subplot, showing the details of the comparison. It should be noted that the measurement data are presented as they are in this study. In consideration of noise, driving environment, data recording, and effect of CAN signals, the simulation and measurement resemble well.

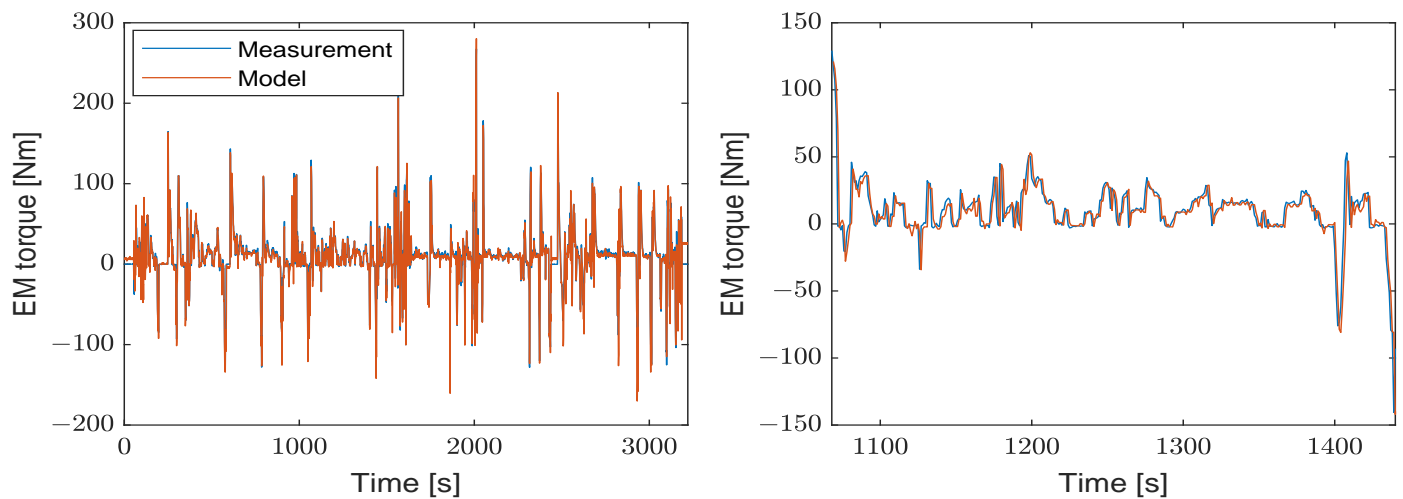


Figure A1. Validation of the EM torque for the ICDC.

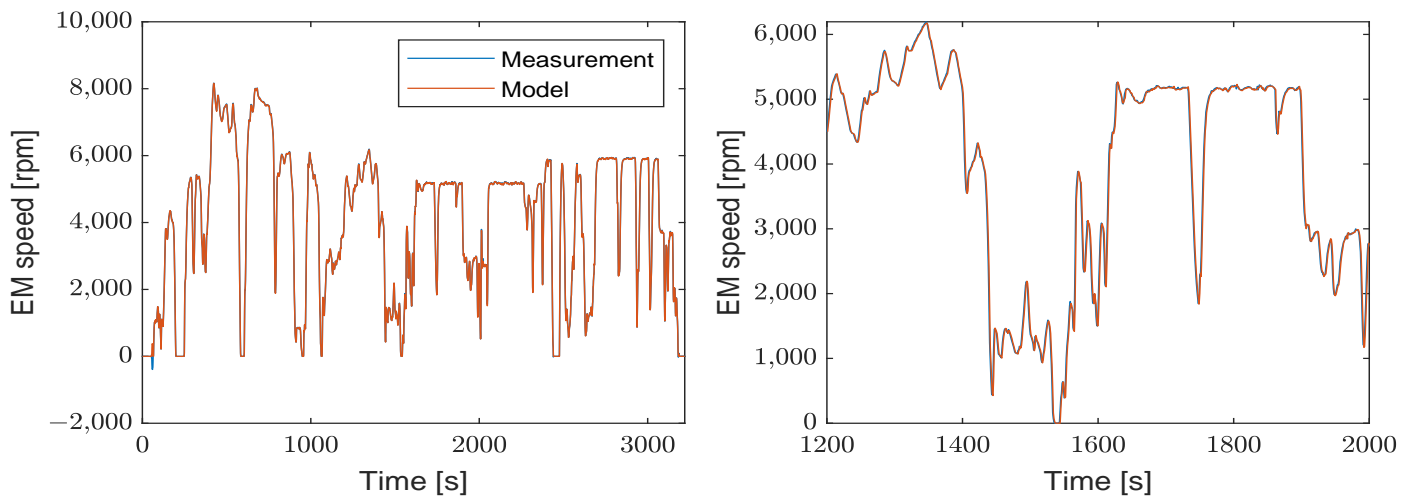


Figure A2. Validation of the EM speed for the ICDC.

The mechanical power of the EM is then given by

$$P_m(k) = \tau_m(k) \omega_m(k). \tag{A8}$$

An efficiency map is used to calculate the power losses of the EM, as shown in Figure A3. This efficiency map includes the effect of the DC-AC inverter. The EM power dissipation is described as a function of its torque and speed, that is,

$$P_{m,loss}(k) = P_{m,loss}(\tau_m(k), \omega_m(k)). \tag{A9}$$

Therefore, the electrical power supplied to/by the EM is expressed as

$$P_{m,el}(k) = P_m(k) + P_{m,loss}(k). \tag{A10}$$

The EM torque and speed are bounded by

$$\tau_m(k) \in [\underline{\tau}_m(\omega_m(k)), \bar{\tau}_m(\omega_m(k))], \tag{A11}$$

$$\omega_m(k) \in [\underline{\omega}_m, \bar{\omega}_m]. \tag{A12}$$

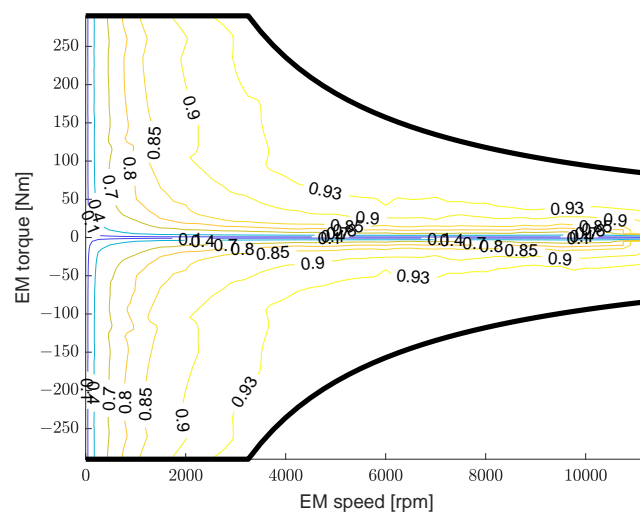


Figure A3. Efficiency map of the EM including the DC-AC inverter.

Appendix A.4. Thermal EM-SST Model

The SST ($P_{s,loss}$) and EM ($P_{m,loss}$) power losses appear as heat, which is removed by a TMS, as demonstrated in Figure A4. The EM and the SST are physically attached. The SST is cooled based on oil splashing, where its heat is taken away by the EM cooling medium indirectly and the ambient air directly due to convection. The EM dissipates heat to the ambient air. Moreover, the cooling medium driven by a pump removes heat from the EM. When the EM temperature is higher than a predefined threshold, the EM is cooled down with a radiator. The goal of the TMS is to maintain the EM temperature below its prescribed thermal limit. A lumped-parameter method is used to capture the thermal behavior of the EM and SST. On the basis of first principles, the thermal EM-SST model is described by

$$c_m m_m \dot{\theta}_m(k) = P_{m,loss}(k) - h_m A_m (\theta_m(k) - \theta_o(k)) - k_m (\theta_m(k) - \theta_s(k)) - h_a A_a (\theta_m(k) - \theta_a), \quad (A13)$$

$$c_f m_f \dot{\theta}_o(k) = h_m A_m (\theta_m(k) - \theta_o(k)) - \phi_f c_f (\theta_o(k) - \theta_i(k)), \quad (A14)$$

$$c_h c_s m_s \dot{\theta}_s(k) = P_{s,loss}(k) + k_m (\theta_m(k) - \theta_s(k)) - h_c A_c (\theta_s(k) - \theta_a), \quad (A15)$$

$$c_f m_f \dot{\theta}_i(k) = \phi_f c_f (\theta_o(k) - \theta_i(k)) - \epsilon \phi_a(k) c_a (\theta_o(k) - \theta_a). \quad (A16)$$

The thermal EM-SST model is validated by measurement data. Since the SST temperature is not available in the CAN data, the EM temperature is used for validation. The measurement data are extracted from the CAN signal regarding the EM temperature of the VCU in the series production vehicle driven on the ICDC. The estimated thermal parameters are provided in Table A1. As shown in Figure A5, a good resemblance can be seen between the model and measurement.

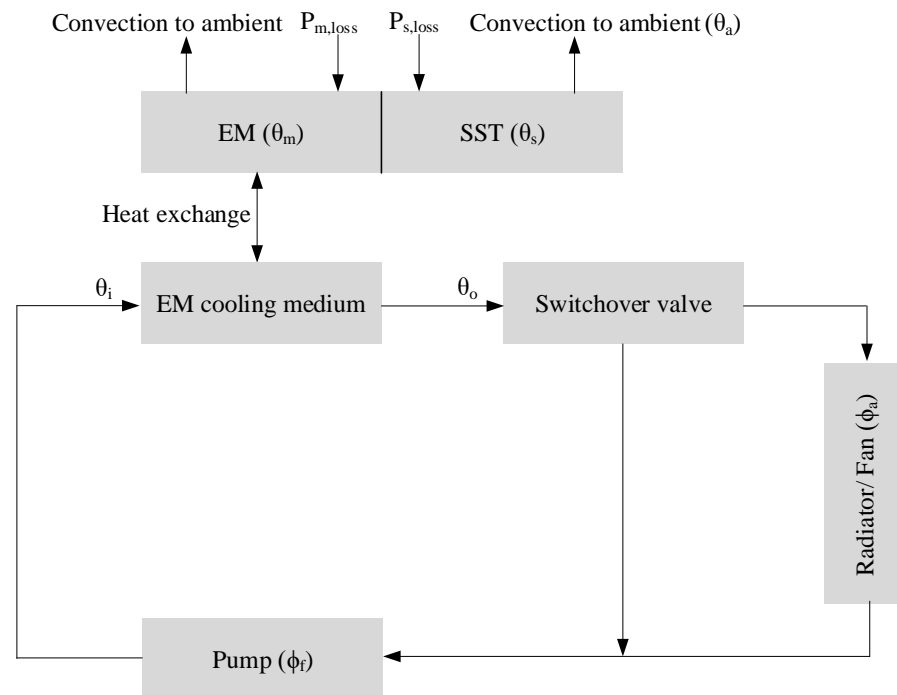


Figure A4. Thermal management architecture for the EM-SST.

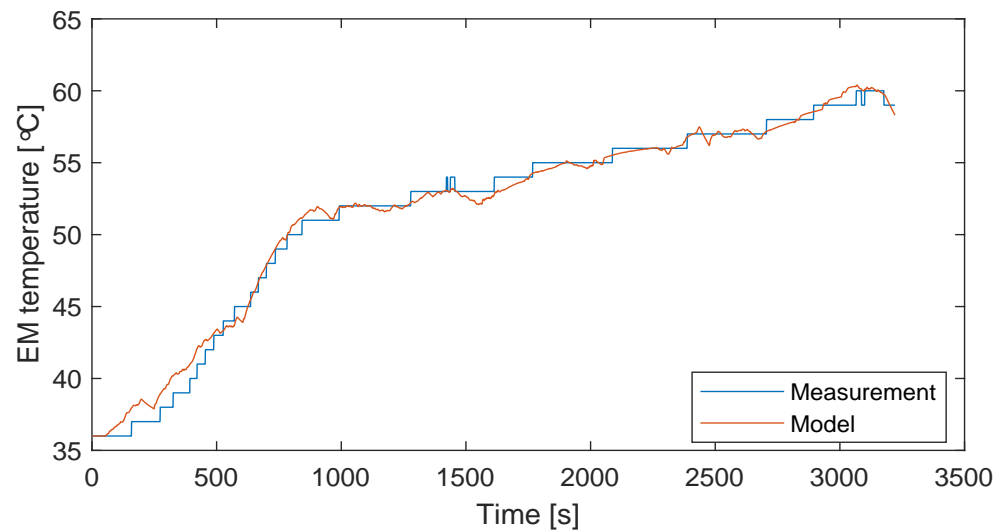


Figure A5. Validation of the EM temperature for the ICDC.

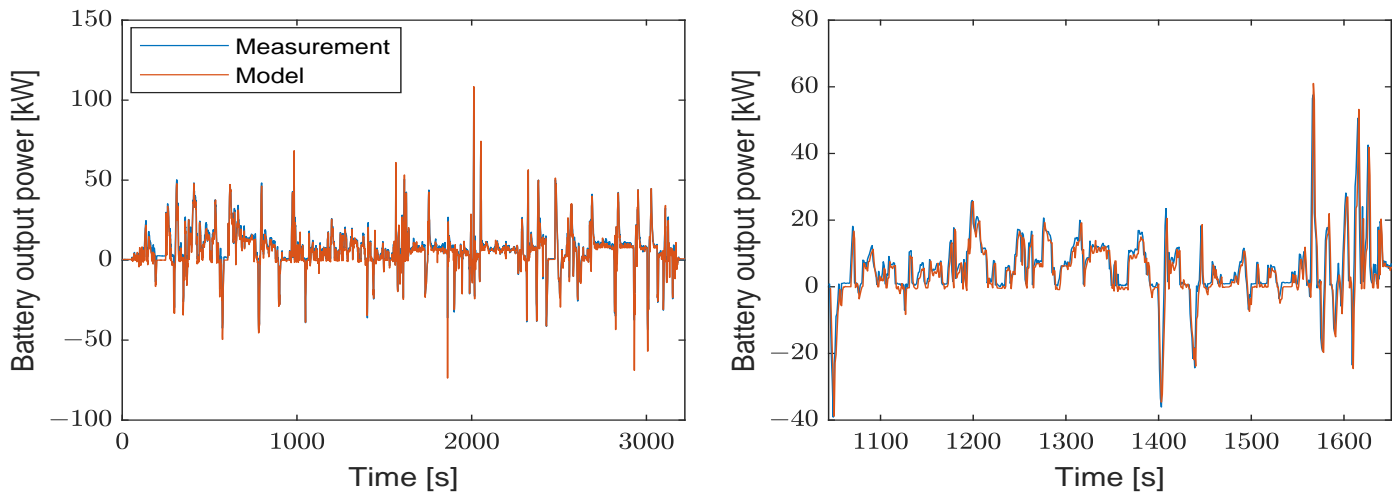


Figure A6. Validation of the battery output power for the ICDC.

Appendix A.5. Battery

The battery provides the power required by the EM, that is,

$$P_b(k) = P_{m,el}(k), \quad (A17)$$

$$\dot{E}_b(k) = -P_b(k). \quad (A18)$$

For the same inputs from the ICDC, the battery output power from the model is compared to the corresponding CAN signal regarding the battery output power in terms of voltage and current (measurement). The comparison can be seen in Figure A6, where the right subplot zooms in on the left subplot. It can be observed that the model and measurement resemble well.

In summary, the SST-based EV model represented by S_1 is validated against the measurement data, which replicates the physical behavior of the series production vehicle in reality.

Appendix B. CVT-Based EV Model

As presented in Section 1, a CVT-based EV model (S_2) is created based on S_1 (Appendix A). The main difference is that the SST model as described in Appendix A.2 is replaced by a

CVT model. The SST mass in (A1) is replaced by \bar{m}_c (Table 1). The thermal model is the same as that in Section 3.7. All the other component models remain the same as S_1 .

In this context, the variator of the pushbelt CVT has two pulleys, a primary pulley (subscript “p”) and a secondary pulley (subscript “s”), which are connected by a pushbelt. The CVT provides a continuous variable speed ratio γ_v between the primary pulley and the secondary pulley. It permits the EM speed to be independent of the wheel speed to optimize its operating point. Given the required torque τ_w (A1) and speed ω_w (A2) at the wheels, the torque and speed of the primary pulley are obtained by

$$\tau_p(k) = \begin{cases} \frac{\tau_w(k)}{\eta_f \gamma_v(k)}, & \text{if } \tau_w(k) > 0, \\ \frac{\eta_f \tau_w(k)}{\gamma_v(k)}, & \text{if } \tau_w(k) \leq 0, \end{cases} \quad (\text{A19})$$

$$\omega_p(k) = \gamma_v(k) \omega_w(k), \quad (\text{A20})$$

The total torque input to the CVT is thus given by

$$\tau_c(k) = \tau_p(k) + \tau_{c,\text{loss}}(k), \quad (\text{A21})$$

where $\tau_{c,\text{loss}}$ represents the torque loss in the CVT, which is described by a lookup table, that is,

$$\tau_{c,\text{loss}}(k) = \tau_{c,\text{loss}}(\tau_p(k), \omega_p(k), \gamma_v(k)). \quad (\text{A22})$$

The power losses of the CVT can thus be calculated by

$$P_{c,\text{loss}}(k) = \tau_{c,\text{loss}}(\tau_p(k), \omega_p(k), \gamma_v(k)) \omega_p(k). \quad (\text{A23})$$

The primary torque and speed ratio are constrained by

$$\tau_p(k) \in [\underline{\tau}_p, \bar{\tau}_p], \quad (\text{A24})$$

$$\gamma_v(k) \in [\underline{\gamma}_v, \bar{\gamma}_v], \quad (\text{A25})$$

where $\underline{\gamma}_v$ is the overdrive ratio and $\bar{\gamma}_v$ the underdrive ratio. Bounds on the primary speed will be implicitly taken into consideration in the constraints on the EM speed. Additionally, to maintain the CVT speed ratio γ_v , the corresponding hydraulic actuation power can be calculated.

Appendix C. Convex Programming

CP demands all the models to be convex. A brief introduction to CP is given here, and interested readers are referred to [22] for a rigorous treatment. A convex optimization problem can be formulated as follows:

$$\begin{aligned} \min \quad & f_0(x), \\ \text{s.t.} \quad & f_i(x) \leq 0, \quad i = 1, \dots, m, \\ & h_j(x) = A_j^T(x) - B_j = 0, \quad j = 1, \dots, n, \end{aligned} \quad (\text{A26})$$

where $f_i(x)$ are convex functions and $h_j(x)$ are affine functions. The feasible set of this optimization problem is convex with m convex sublevel sets and n hyperplanes. A convex function can be described as

$$f(\beta x_1 + (1 - \beta) x_2) \leq \beta f(x_1) + (1 - \beta) f(x_2), \quad (\text{A27})$$

where $\beta \in [0, 1]$, and it means that the line segment between any two points lies above the graph. Models that are originally non-convex can be reformulated based on approximations, relaxations, and change of variables. Model convexity can be verified, by using basic convex functions, for example, linear functions, quadratic functions, quadratic-over-

linear functions and opposite of geometric mean functions, and operations that preserve convexity, such as nonnegative weighted sums and pointwise maximum.

Appendix D. Main Parameters of EV Model

The main EV model parameters are provided in the following table, including vehicle parameters with reference to the series production vehicle and validated thermal parameters.

References

1. Kwon, K.; Seo, M.; Min, S. Efficient Multi-Objective Optimization of Gear Ratios and Motor Torque Distribution for Electric Vehicles with Two-Motor and Two-Speed Powertrain System. *Appl. Energy* **2020**, *259*, 114190. [[CrossRef](#)]
2. Karki, A.; Phuyal, S.; Tuladhar, D.; Basnet, S.; Shrestha, B. P. Status of Pure Electric Vehicle Power Train Technology and Future Prospects. *Appl. Syst. Innov.* **2020**, *3*, 35. [[CrossRef](#)]
3. Han, J.; Shin, J.; Kim, J.; Oh, S. Design 2-Speed Transmission for Compact Electric Vehicle Using Dual Brake System. *Appl. Sci.* **2019**, *9*, 1793. [[CrossRef](#)]
4. Hupkes, I. Variable Drive EV: Comfort Solution for Full Electric Vehicles. In Proceedings of the 3rd International VDI Conference: CVT in Automotive Applications, Baden-Baden, Germany, 19–20 March 2019.
5. Anselma, P. G.; Belingardi, G. Comparing Battery Electric Vehicle Powertrains through Rapid Component Sizing. *Int. J. Electr. Hybrid Veh.* **2019**, *11*, 36–58. [[CrossRef](#)]
6. Van der Sluis, F.; Römers, L.; van Spijk, G.; Hupkes, I. CVT, *Promising Solutions for Electrification*; SAE Technical Paper 2019-01-0359; SAE International: Warrendale, PA, USA, 2019.
7. Wei, C.; Hofman, T.; Ilhan Caarls, E.; van Iperen, R. A Review of the Integrated Design and Control of Electrified Vehicles. *Energies* **2020**, *13*, 5454. [[CrossRef](#)]
8. Silvas, E.; Hofman, T.; Murgovski, N.; Etman, L.F.P.; Steinbuch, M. Review of Optimization Strategies for System-Level Design in Hybrid Electric Vehicles. *IEEE Trans. Veh. Technol.* **2017**, *66*, 57–70. [[CrossRef](#)]
9. Singh, K.V.; Bansal, H.O.; Singh, D. Feed-forward Modeling and Real-time Implementation of an Intelligent Fuzzy Logic-based Energy Management Strategy in a Series-parallel Hybrid Electric Vehicle to Improve Fuel Economy. *Electr. Eng.* **2020**, *102*, 967–987. [[CrossRef](#)]
10. Lee, H.; Song, C.; Kim, N.; Cha, S.W. Comparative Analysis of Energy Management Strategies for HEV: Dynamic Programming and Reinforcement Learning. *IEEE Access* **2020**, *8*, 67112–67123. [[CrossRef](#)]
11. Qi, Z.; Shi, Q.; Zhang, H. Tuning of Digital PID Controllers Using Particle Swarm Optimization Algorithm for a CAN-Based DC Motor Subject to Stochastic Delays. *IEEE Trans. Ind. Electron.* **2020**, *67*, 5637–5646. [[CrossRef](#)]
12. Zhang, Y.; Wang, S.; Ji, G. A Comprehensive Survey on Particle Swarm Optimization Algorithm and Its Applications. *Math. Probl. Eng.* **2015**, *2015*, 931256. [[CrossRef](#)]
13. Pourabdollah, M.; Silvas, E.; Murgovski, N.; Steinbuch, M.; Egardt, B. Optimal Sizing of a Series PHEV: Comparison between Convex Optimization and Particle Swarm Optimization. *IFAC-PapersOnLine* **2015**, *48*, 16–22. [[CrossRef](#)]
14. East, S.; Cannon, M. Energy Management in Plug-In Hybrid Electric Vehicles: Convex Optimization Algorithms for Model Predictive Control. *IEEE Trans. Control Syst. Technol.* **2020**, *28*, 2191–2203. [[CrossRef](#)]
15. Pourabdollah, M.; Murgovski, N.; Grauers, A.; Egardt, B. Optimal Sizing of a Parallel Phev Powertrain. *IEEE Trans. Veh. Technol.* **2013**, *62*, 2469–2480. [[CrossRef](#)]
16. Wei, C.; Hofman, T.; Ilhan Caarls, E.; van Iperen, R. Evolution and Classification of Energy and Thermal Management Systems in Electrified Powertrains. In Proceedings of the 2019 IEEE Vehicle Power and Propulsion Conference, Hanoi, Vietnam, 14–17 October 2019.
17. Luin, B.; Petelin, S.; Al-Mansour, F. Microsimulation of Electric Vehicle Energy Consumption. *Energy* **2019**, *174*, 24–32. [[CrossRef](#)]
18. Wei, C.; Hofman, T.; Ilhan Caarls, E.; van Iperen, R. Integrated Energy and Thermal Management for Electrified Powertrains. *Energies* **2019**, *12*, 2058. [[CrossRef](#)]
19. Markel, T.; Brooker, A.; Hendricks, T.; Johnson, V.; Kelly, K.; Kramer, B.; O’Keefe, M.; Sprik, S.; Wipke, K. ADVISOR: A Systems Analysis Tool for Advanced Vehicle Modeling. *J. Power Sources* **2002**, *110*, 255–266. [[CrossRef](#)]
20. Ruan, J.; Walker, P.; Zhang, N. A Comparative Study Energy Consumption and Costs of Battery Electric Vehicle Transmissions. *Appl. Energy* **2016**, *165*, 119–134. [[CrossRef](#)]
21. Murgovski, N.; Johannesson, L.; Sjöberg, J. Convex Modeling of Energy Buffers in Power Control Applications. *IFAC Proc. Vol.* **2012**, *45*, 92–99. [[CrossRef](#)]
22. Boyd, S.; Vandenberghe, L. *Convex Optimization*; Cambridge University Press: Cambridge, UK, 2009.
23. van Berkel, K. Control of a Mechanical Hybrid Powertrain. Ph.D. Thesis, Eindhoven University of Technology, Eindhoven, The Netherlands, 2013.
24. van der Sluis, F. The Pushbelt designed for Change. In Proceedings of the 3rd International VDI Conference: CVT in Automotive Applications, Baden-Baden, Germany, 19–20 March 2019.

25. van der Sluis, F.; Yildiz, S.; Brandsma, A.; Veltmans, P.; Kunze, M. The CVT Pushbelt reinvented for Future Compact and Efficient Powertrains. In Proceedings of the 2017 JSAE Annual Congress, Yokohama, Japan, 24–26 May 2017.
26. Pourabdollah, M. Optimization of Plug-in Hybrid Electric Vehicles. Ph.D. Thesis, Chalmers University of Technology, Gothenburg, Sweden, 2015.
27. *Electrical and Electronics Technical Team Roadmap*; Technical Report; U.S. DRIVE: Washington, DC, USA, 2017.
28. Lutsey, N.; Nicholas, M. *Update on Electric Vehicle Costs in the United States through 2030*; Technical Report; International Council on Clean Transportation: Washington, DC, USA, 2019.
29. Mahmoudzadeh Andwari, A.; Pesiridis, A.; Rajoo, S.; Martinez-Botas, R.; Esfahanian, V. A Review of Battery Electric Vehicle Technology and Readiness Levels. *Renew. Sustain. Energy Rev.* **2017**, *78*, 414–430. [[CrossRef](#)]
30. Software for Disciplined Convex Programming. Available online: <http://cvxr.com/> (accessed on 11 February 2021).
31. Tang, T.; Devlin, M.; Mathur, N.; Henly, T.; Saathoff, L. Lubricants for (Hybrid) Electric Transmissions. *SAE Int. J. Fuels Lubr.* **2013**, *6*, 289–294. [[CrossRef](#)]
32. McFadden, C.; Hughes, K.; Raser, L.; Newcomb, T. Electrical Conductivity of New and Used Automatic Transmission Fluids. *SAE Int. J. Fuels Lubr.* **2016**, *9*, 519–526. [[CrossRef](#)]
33. Bennion, K.; Moreno, G. Convective Heat Transfer Coefficients of Automatic Transmission Fluid Jets with Implications for Electric Machine Thermal Management. In Proceedings of the ASME 2015 International Technical Conference and Exhibition on Packaging and Integration of Electronic and Photonic Microsystems InterPACK2015, San Francisco, CA, USA, 6–9 July 2015.
34. Salah, M. Nonlinear Control Strategies for Advanced Vehicle Thermal Management Systems. Ph.D. Thesis, Clemson University, Clemson, SC, USA, 2007.